Development of a generic adenovirus delivery system based on structure-guided design of bispecific trimeric DARPin adapters

Birgit Dreier[a], Annemarie Honegger[a], Christian Hess[a], Gabriela Nagy-Davidescu[a], Peer R. E. Mittl[a], Markus G. Grütter[a], Natalya Belousova[b], Galina Mikheeva[b], Victor Krasnykh[b], and Andreas Plückthun[a,1]

[a]Department of Biochemistry, University of Zurich, CH-8057 Zurich, Switzerland; and [b]Department of Experimental Diagnostic Imaging, M.D. Anderson Cancer Center, University of Texas, Houston, TX 77030

Edited by Stephen C. Harrison, Children's Hospital, Harvard Medical School, and Howard Hughes Medical Institute, Boston, MA, and approved January 17, 2013 (received for review August 9, 2012)

Adenoviruses (Ads) have shown promise as vectors for gene delivery in clinical trials. Efficient viral targeting to a tissue of choice requires both ablation of the virus' original tropism and engineering of an efficient receptor-mediated uptake by a specific cell population. We have developed a series of adapters binding to the virus with such high affinity that they remain fully bound for >10 d, block its natural receptor binding site and mediate interaction with a surface receptor of choice. The adapter contains two fused modules, both consisting of designed ankyrin repeat proteins (DARPins), one binding to the fiber knob of adenovirus serotype 5 and the other binding to various tumor markers. By solving the crystal structure of the complex of the trimeric knob with three bound DARPins at 1.95-Å resolution, we could use computer modeling to design a link to a trimeric protein of extraordinary kinetic stability, the capsid protein SHP from the lambdoid phage 21. We arrived at a module which binds the knob like a trimeric clamp. When this clamp was fused with DARPins of varying specificities, it enabled adenovirus serotype 5-mediated delivery of a transgene in a human epidermal growth factor receptor 2-, epidermal growth factor receptor-, or epithelial cell adhesion molecule-dependent manner with transduction efficiencies comparable to or even exceeding those of Ad itself. With these adapters, efficiently produced in *Escherichia coli*, Ad can be converted rapidly to new receptor specificities using any ligand as the receptor-binding moiety. Prefabricated Ads with different payloads thus can be retargeted readily to many cell types of choice.

protein design | tumor targeting | viral retargeting | X-ray crystallography | protein engineering

Adenoviruses (Ads) are actively being developed as vectors for in vivo gene delivery to diagnose and treat human disease. They can incorporate up to 35 kb of foreign DNA, are safe because they do not integrate into the host cell genome, and can infect dividing and nondividing cells (1–3). However, achieving efficient and specific gene transfer to disease-affected tissues by Ads constitutes an enormous technological challenge, because Ads—like any other virus—lack specificity for diseased tissues. Furthermore, regardless of the delivery route, Ads undergo numerous interactions with nontarget, normal tissues, including cellular and molecular components of the immune system.

The challenge in efficient and highly specific retargeting of Ads thus lies in ablating the Ads' natural interactions and facilitating uptake of the virus by the cell population or tissue of choice in a highly specific manner.

Ad capsids are composed of three major proteins, the hexon that forms the shell of the capsid, the penton base, and the fiber that associates with the penton base to form the penton capsomers. The entrance of Ads into the cell first requires the interaction of the knob domain of the fiber with a primary receptor on the target cell. The best-studied and most frequently used serotype, Ad5, binds to the Coxsackievirus-and-Ad receptor (CAR) (4, 5), but other serotypes use different primary receptors, such as sialic acid, CD46, desmoglein 2, CD80, or CD86 (6–9). Independent of the type of primary receptor, in a second step the penton base of the Ad makes contact with integrin receptors on the cell surface, initiating the subsequent uptake of the virus by receptor-mediated endocytosis (10; for review see refs. 11 and 12).

For efficient targeting of Ad5, a first major task is to ablate the virion's natural tropism, and this ablation has been achieved by introducing mutations into the knob, hexon, and/or penton base within motifs mediating interactions with cell-surface molecules or blood components, leading to reduced transduction efficiency (13–19). The second challenge is to retarget the Ad5 specifically to the diseased cells/tissue. Because the natural receptor usually is expressed at low levels in the desired cell populations or might not be accessible in the tissue because of the polarity of CAR expression and the localization to difficult-to-reach tight junctions (20), the virus must be tagged with a new specificity for receptors that are expressed on cells in the diseased tissue.

To retarget Ad5, two types of strategies have been followed: the genetic fusion to Ad coat proteins, mainly established for fiber fusions (16, 21–25), and the development of bispecific adapters (for review see refs. 14 and 26).

A strategy of creating a generic, universal bispecific adapter without the need to produce new virus for every new receptor target seems compelling. Previously we and others have reported the use of bispecific adapters binding to a virus capsid protein for specific adenovirus-mediated targeting (14, 26–37). The successful execution of the adapter strategy depends critically on our ability to design protein adapters for Ad that allow the targeting of any desired disease-associated receptor and whose association with the Ad virion is highly stable and can be fine-tuned to be compatible with the virion's structural integrity and its stepwise disintegration during cell entry (38).

As an important step in this technology development, we have designed adapters derived from a trimeric clamp that associates virtually irreversibly with Ad virions. To do so, we exploited unique properties of designed ankyrin repeat proteins (DARPins) that had been selected to bind the mutant Ad5 knobΔTAYT (37).

Author contributions: B.D., A.H., and A.P. designed research; B.D., C.H., G.N.-D., P.R.E.M., N.B., and G.M. performed research; B.D., A.H., C.H., G.N.-D., P.R.E.M., M.G.G., V.K., and A.P. analyzed data; and B.D., A.H., P.R.E.M., V.K., and A.P. wrote the paper.

Conflict of interest statement: A.P. is a shareholder of Molecular Partners AG, which is commercializing the DARPin technology.

This article is a PNAS Direct Submission.

Data deposition: Crystallography, atomic coordinates, and structure factors reported in this paper have been deposited in the Protein Data Bank, www.pdb.org (ID code 4ATZ).

[1]To whom correspondence should be addressed. E-mail: plueckthun@bioc.uzh.ch.

See Author Summary on page 3725 (volume 110, number 10).

This article contains supporting information online at www.pnas.org/lookup/suppl/doi:10.1073/pnas.1213653110/-/DCSupplemental.

We solved the crystal structure of the DARPin/knob complex at 1.95-Å resolution. We designed a molecule based on this result in which the knob-binding DARPins were trimerized using an unusually stable trimerization domain, SHP of the lambdoid phage 21. As a result, these trimeric fusion proteins clamp the knob so tightly that they become an integral structural component of the virus. Importantly, however, as our transduction studies showed, this highly stable association is fully compatible with virus disintegration during targeted infection. By fusing this clamp genetically to DARPins specific for biomarkers of human tumors, we could achieve specific transduction of cells expressing the tumor cell markers human epidermal growth factor receptor 2 (HER2), epithelial cell adhesion molecule (EpCAM), or epidermal growth factor receptor (EGFR).

Results

For efficient retargeting of Ad using an adapter-based strategy, it is crucial to develop adapters that have such a high affinity to the virion that they essentially do not dissociate at all from the virus particle for several days. Previously, we described an approach to develop an adapter based on DARPins: One type of DARPin that was selected to bind the Ad5 knob (37) was arranged as a linear multimer to wrap around the Ad5 knob and fused to another retargeting DARPin specific for HER2. This adapter was shown to enable transduction of HEK293 cells overexpressing HER2 with the Ad–adapter complex. However, the system showed increased efficiency only at higher than stoichiometric ratios, with an excess of adapter over knob, for mono- and divalent adapters, thus suggesting some dissociation. Also, a trivalent DARPin offered no further improvement over a divalent DARPin, probably because not all knob subunits could be occupied in the linear arrangement of knob-binding DARPins and therefore affinity was not increased further. To create even more tightly binding adapters, we solved the crystal structure of a knob-binding DARPin in complex with the Ad5 knob and used this structure as the basis for designing a tightly binding trimer clamping the trimeric structure of the knob.

Structure Determination of Ad5 Knob/Darpin 1D3 Complex. To aid the design of improved adapters, the exact positioning of the DARPin 1D3 on the knobΔTAYT was determined by X-ray crystallography of the complex. The complex crystallized in space group $P2_12_12_1$ with six polypeptide chains in the asymmetric unit (Table S1). The 1.95-Å resolution crystal structure revealed an exact 3:1 stoichiometry with three DARPin 1D3 molecules binding to one Ad5 knob trimer (Fig. 1 *A* and *B*).

Although all three 1D3 DARPins were well defined in the final electron density maps (Fig. S1), the analysis of their B-factors, a measure of thermal stability, revealed pronounced differences. The average B-factors for the Ad5 knob trimer with chain labels A, B, and C are 32.6, 34.0, and 41.2 $Å^2$; for the cognate DARPins with chain labels D, E, and F these values are 45.2, 51.1, and 69.3 $Å^2$, respectively. Thus, the average B-factor is significantly higher for DARPin F than for the others. This observation could be explained by either a lower occupancy, which would indicate that the Ad5 knob trimer cannot bind three DARPins simultaneously, or elevated thermal mobility caused by fewer contacts with neighboring molecules that are related by crystallographic symmetry. The analysis of the crystal lattice revealed that, in addition to the main interface contact with the Ad5 knob, DARPin chains D, E, and F also are involved in crystal contacts but with very different buried surface areas of 617, 900, and 42.4 $Å^2$, respectively. Thus, DARPin chain F is fixed only loosely in the crystal lattice, explaining its increased average B-factor.

Previously, we observed that even at high concentrations DARPin 2E6 on average would bind with only 2.5 molecules to one Ad5 knob trimer in solution (37). DARPins 1D3 and 2E6 are closely related. They share identical interface residues and differ in just three framework positions outside the DARPin/Ad5 knob interface. Thus, it appears that binding to the trimeric knob has some inherent asymmetry.

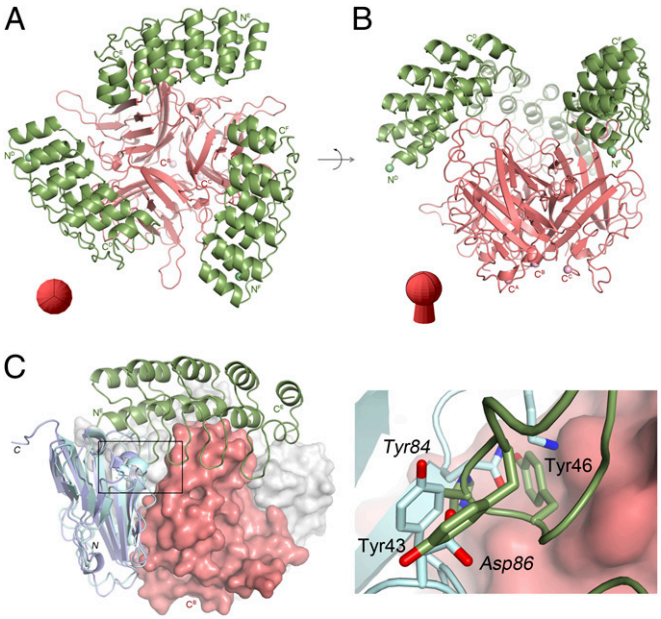

Fig. 1. Crystal structure of Ad5 knob/1D3 complex. Overview of the complex showing the Ad5 knob and DARPin 1D3 molecules in two perpendicular orientations as red and green ribbons, respectively. (*A*) Top view. (*B*) Side view. The orientation of the fiber knob is shown schematically in red. (*C*) Superposition of the Ad5 knob/1D3 complex with the CAR D1 domain of Ad37 (PDB ID: 2J12; light blue ribbon) or CAR D1 from Ad12 (PDB ID: 1KAC; violet ribbon). The Ad5 knob trimer is shown as red and gray surfaces, and the Ad37 and Ad12 knobs have been omitted. Only one chain of the 1D3 DARPin is shown in green. The boxed area is magnified on the right. Here green and light blue sticks indicate residues from 1D3 and CAR D1, respectively. Labels in roman and italic characters refer to 1D3 and CAR D1, respectively.

The epitope to which 1D3 binds is located on the side opposite the Ad5 knob N terminus (where the fiber shaft is located) and fairly close to the threefold trimer axis (Fig. 1 and Fig. S2). The observed arrangement illustrates that 1D3 can recognize the full-length knob protein in the context of the Ad5 virion, as previously shown (37). Furthermore, the ΔTAYT deletion (residues 489–492), which has been reported to abolish CAR binding (39, 40), is located close to the Ad5 knob's N terminus and shaft and hence remote from the 1D3 epitope. Therefore, 1D3 does not discriminate between WT and ΔTAYT isoforms of Ad5 knob (37). Furthermore, we predicted from the structure that binding of 1D3 to the knob would interfere directly with CAR binding to the WT knob. Mapping of the 1D3- and CAR-binding sites on the knob revealed that, even though the two epitopes are not fully overlapping, binding of CAR to the Ad5 knob/1D3 complex would create a clash between residues 13–19 and 43–46 from 1D3 and residues 62–65 and 84–86 from CAR (Fig. 1*C*). This inference was borne out by direct inhibition experiments (see below).

Most importantly, the structure of the Ad5 knobΔTAYT/1D3 complex aids in the design of improved recognition modules. In the complex, the C termini of the DARPins point away from Ad5 surface and are in an almost perfect triangular arrangement with a distance between them of ∼48 Å. Because of this configuration, we reasoned that the stability of the knob–DARPin complex could be improved by fusing three DARPins with a very stable trimerization module that supports exactly this spacing and orientation of bound DARPins on the knob without any additional flexibility. This fusion should result in a clamp with very high avidity.

Construction of Trimeric Adapters by Rational Design. To test this reasoning, we chose to design a highly stable trimeric module to

link three copies of the knob-binding DARPin 1D3 in an optimal arrangement to clamp the knob. First, the consensus C-capping repeat (C-cap) of the knob-binding DARPin was replaced by a C-cap of higher thermal stability and fewer structural fluctuations, as previously reported (41, 42). This approach seemed reasonable, because the C-cap was not involved in directly binding to the knob, and, indeed, with the new C-cap no differences in affinity were observed (Fig. S3).

Because the crystal structure showed that the C termini of the three knob-bound DARPins point away from the virus, we fused these termini to the small 11.8-kDa capsid protein SHP of the lambdoid phage 21, whose crystal structure we had previously determined (43). This protein forms a highly stable trimer that remains intact even in SDS gels and which dissociates and denatures with a half-life of 1 mo in solution (43). According to our design, this trimeric structure containing SHP was expected to be located above the knob, with the three DARPins grabbing the knob from three sides (Fig. 2 and Fig. S4). We reasoned that this clamp concept would work most efficiently when the linkers are as short as possible without leading to steric interference, to provide the highest local concentration of correctly oriented DARPins. To optimize the design, three variants of different lengths of the minimal linker between the knob-binding DARPin 1D3nc ("nc" for new cap) and SHP were constructed (Fig. 2 and Fig. S4). All these fusions were expressed in *Escherichia coli* and formed trimers even in the absence of a knob. This trimerization was quantitative, because no monomer peak could be detected using size-exclusion chromatography in combination with multiangle static light scattering (SEC-MALS). The trimers bound to the trimeric knob with a perfect 1:1 stoichiometry as determined by MALS (Fig. S5), in accordance with three DARPins binding to the three knob subunits. We did not observe cross-linking of knob proteins by the trimeric knob-binding modules, consistent with a clamp-like binding, thus eliminating the danger of virus cross-linking in later transduction experiments.

Trimeric Adapters Conferred Ad-Mediated Gene Transfer in a HER2-Dependent Manner. The potential of the 1D3nc_SHP knob-binding modules in Ad5-mediated gene transfer was investigated. As a model system, we chose to target HER2, a cell-surface receptor overexpressed on many tumor cells. Retargeting DARPins were fused either at the N or C terminus of the 1D3nc_SHP module (Fig. 2 and Fig. S4). Two different HER2-binding DARPins, G3 or 9.29 (44, 45), recognizing epitopes on different domains of the target HER2, or the control DARPin E2_5 (46) were tested. All adapters containing the knob-binding module and a retargeting DARPin could be expressed in high-yield, formed trimers (Fig. S6*A*) and bound both the knob and HER2 simultaneously, as determined by ELISA (Fig. S6*B*).

The purified adapters then were used to form a complex with the Ad5 virus encoding a luciferase reporter gene (Ad5luc), and the complex was used to transduce target cells. The use of Ad5 with an unmodified WT knob allowed evaluation of the CAR-dependent background transduction and comparison of the trimeric adapters to the previously described linear adapter (37). If the trimeric adapter was tightly bound, no CAR-mediated entry should be observed, because crystallographic data predicted that binding of DARPin 1D3 to the knob would block the knob from binding to CAR (Fig. 1*C*) (47). Indeed, this prediction was confirmed in competition experiments (Fig. S7) with the human CAR D1 domain, which interacts with the WT Ad5 knob domain.

The binding of adapter or CAR also was mutually exclusive in transduction of HEK293 Flp-In cells expressing high levels of CAR: At a ratio of one trimeric 1D3nc_SHP1 knob-binding clamp per trimeric knob, transduction with Ad5luc was blocked completely and could not be reduced further by a 10-fold excess of 1D3nc_SHP1 to knob (Fig. S8).

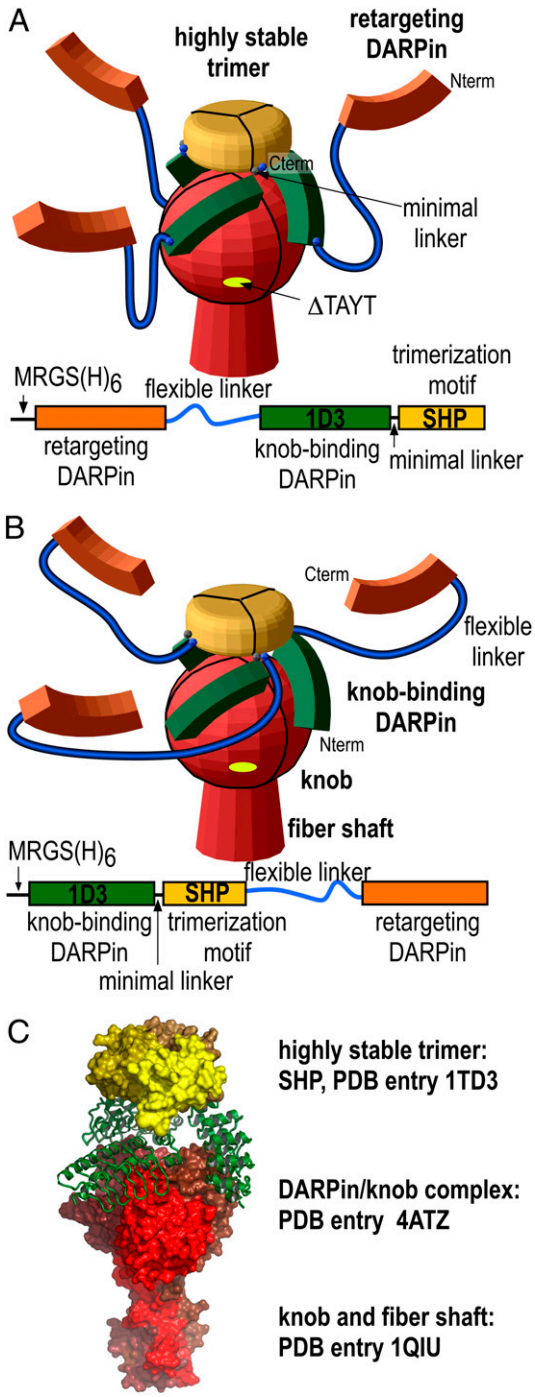

Fig. 2. Construction of the trimeric clamp based on the crystal structure of the DARPin/knob complex. (*A* and *B*) Schematic representation of the two trimeric adapter complexes. The retargeting DARPins (orange) are fused via a long flexible linker (blue) to either the N terminus (*A*) or C terminus (*B*) of the knob-binding DARPin (green). The knob-binding DARPin is fused in turn by a very short minimal linker (blue dot) to the trimerization module (yellow), SHP from the lambdoid phage 21. The fusion of the knob-binding DARPin was always at the N terminus of SHP, which is on the same face and very close to the C terminus. Three variants of minimal linkers were used: SHP1 containing a single glycine (G), SHP2 containing the dipeptide glycine-alanine (GA), or SHP3 containing the 10 amino acids GLKAGADVNA. The knob and fiber shaft are shown in red. Below the model, the respective gene is shown schematically. (*C*) Detailed structural model with an indication of the experimental structures on which it is based (PDB ID: 4ATZ, this work).

To investigate HER2-mediated transduction, Ad5luc was coated with the HER2-retargeting adapter at a ratio of one trimeric adapter to one trimeric knob. This complex was used to transduce HEK293 Flp-In cells stably overexpressing HER2 (293Flp/HER2) or, as control, the parental HEK293 Flp-In cells expressing only low amounts of HER2 (48). The activity of the luciferase was measured 14 h posttransduction (Fig. 3*A*). As evidenced by the difference in reporter expression in control and HER2-expressing cells, HER2-specific transduction was observed for both HER2 binders, G3 and 9.29, regardless of whether they were fused to the N or C terminus of the knob-binding module. However, the G3-based adapter resulted in a 30-fold increase in luciferase expression as compared with the non–CAR-mediated background transduction caused by Ad5 coated with the knob-binding module alone, whereas DARPin 9.29 was only 25- to 27-fold above background. The N-terminal fusion of the DARPin retargeting HER2 to the knob-binding unit seemed to yield higher luciferase units, 25- to 36-fold, compared with 20- to 24-fold of the corresponding C-terminal fusions. In this experimental set-up the different linker spacings between the knob-binding DARPin and SHP seemed to perform equally well.

Next we verified the specificity of the HER2-mediated transduction using a competition assay (Fig. S9). The transduction was specific for HER2, because the luciferase expression could be reduced when the cells were preincubated with the DARPin G3 but not with a control, DARPin E2_5. We observed a high background signal in untransfected HEK293 Flp-In cells with all adapters containing a HER2-specific DARPin. To investigate whether this high background signal resulted from a low level of HER2 expression by the HEK293 Flp-In cells or from reinfection by newly produced virus via CAR, we investigated transduction efficiency in a HER2, CAR, and a system not expression E1 or E3, using the cell lines CHO Flp-In and CHO/HER2 (Fig. S10). Whereas the adapter containing the control DARPin E2_5 did not mediate transduction of any of the two cell lines, the adapter fused to the HER2-binding DARPin G3 mediated transduction

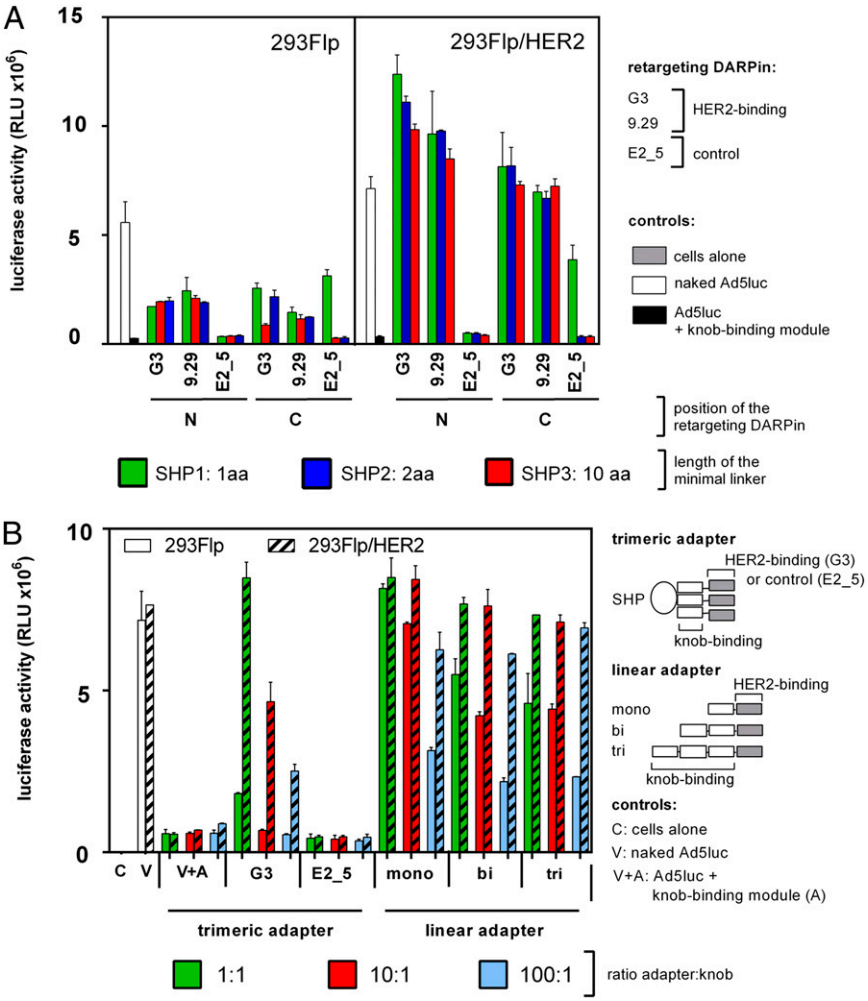

Fig. 3. Comparison of the transduction efficiency of WT Ad5 coated with various DARPin adapters. (*A*) HEK293 Flp-In cells (293Flp) or HEK293 Flp-In stably expressing HER2 (293Flp/HER2) were transduced with a multiplicity of 100 vp per cell coated with a 1:1 ratio of knob-binding DARPin to knob subunits. The trimeric adapter containing the trimeric knob-binding module 1D3nc_SHP1 (green bars), 1D3nc_SHP2 (red bars), or 1D3nc_SHP3 (blue bars) spaced by different linker lengths was fused to a DARPin binding to HER2, G3, or 9.29 or to a control DARPin, E2_5, respectively. These DARPins were fused to the N terminus (N) or C terminus (C) of the trimeric 1D3nc_SHP knob-binding module. (*B*) HEK293 Flp-In cells (293Flp) or HEK293 Flp-In cells stably expressing HER2 (293Flp/HER2) were transduced with 100 vp per cell coated with a 1:1 (green bars), 10:1 (red bars), or 100:1 (blue bars) ratio of knob-binding DARPin to knob subunits. The trimeric knob-binding module 1D3nc_SHP1 was fused to the HER2-binding DARPin G3 or to the control DARPin E2_5. The linear DARPins contained one (mono), two (bi), or three (tri) knob-binding modules in series and one HER2-binding module. Controls were cells alone (C); cells infected with virus alone (white bars; V); or cells infected with virus coated with the trimeric 1D3nc_SHP1 knob-binding module (without the HER2-binding module; V+A). Relative luciferase light units (RLU) were determined 14.5 h after infection. The assay was performed in duplicate; error bars show SD.

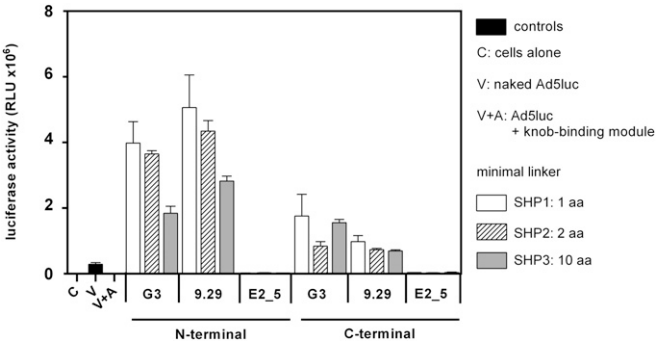

Fig. 4. Transduction of adapter-coated Ad5 into BT474 tumor cells overexpressing HER2. BT474 cells were infected with a multiplicity of 100 vp per cell with a 1:1 ratio of trimeric adapter to knob. The trimerization module containing various minimal linker lengths [1D3nc_SHP1 with 1-aa spacing (white bars), 1D3nc_SHP2 with 2-aa spacing (hatched bars), or 1D3nc_SHP3 with 10-aa spacing (gray bars)] was fused to a DARPin binding to HER2, G3, or 9.29 or to a control DARPin E2_5. These DARPins were fused to either the N terminus or C terminus of the 1D3nc_SHP unit. Black bars indicate controls [C, cells without infection; V, cells infected with virus alone; A, cells infected with virus coated with the trimeric 1D3nc_SHP1 knob-binding module (without the HER2-binding module)]. RLU were determined 16 h after infection. The assay was performed in duplicate; error bars show the SD.

of only the cell line overexpressing HER2 at a level 35-fold above background. As expected, when tested on CHO cells, luciferase expression was observed at the same low levels with either virus alone (i.e, Ad5luc coated with either of the two control adapters, 1D3nc_SHP1 alone or fused to the control DARPin E2_5, as well as with Ad5luc coated with the HER2-specific adapter containing the DARPin G3).

Next, the efficiency of the previously designed linear DARPin-based adapters (37) was compared with that of the trimeric adapters designed in this study (Fig. 3*B*). 293Flp/HER2 or the parental cell line as control was infected with adapter-coated virus at 100 virus particles (vp) per cell with different ratios of adapter to knob. When the trimeric adapters were used, most efficient transduction was achieved at the lowest tested ratio, 1:1, as is consistent with a perfect three DARPin to one knob stoichiometry and very tight binding. At this ratio, transduction of HER2-expressing cells was 15-fold more efficient than non–CAR-mediated background, i.e., Ad coated with the knob-binding module alone not containing an anti-HER2 DARPin. The decrease in luciferase activity with increasing adapter concentration can be explained by gradual saturation of HER2 with free adapters in excess.

The efficacy of transduction of 293Flp/HER2 cells enabled by the linear adapters was nearly equal to that achieved with the trimeric adapters (Fig. 3*B*). However, in the case of linear adapters and WT Ad5 knob proficient in CAR binding, the background signal of luciferase in HEK293 Flp-In cells was elevated and in some cases reached the intensities obtained from 293Flp/HER2 cells. This effect was most dramatic with the linear monovalent 2E6_G5 adapter, which had a much lower affinity than the linear bi- or trivalent 2E6_G5 adapters (37). When the ratio of adapter was increased 10- or 100-fold over knob subunit concentration, this background signal was reduced. Taken together, these two

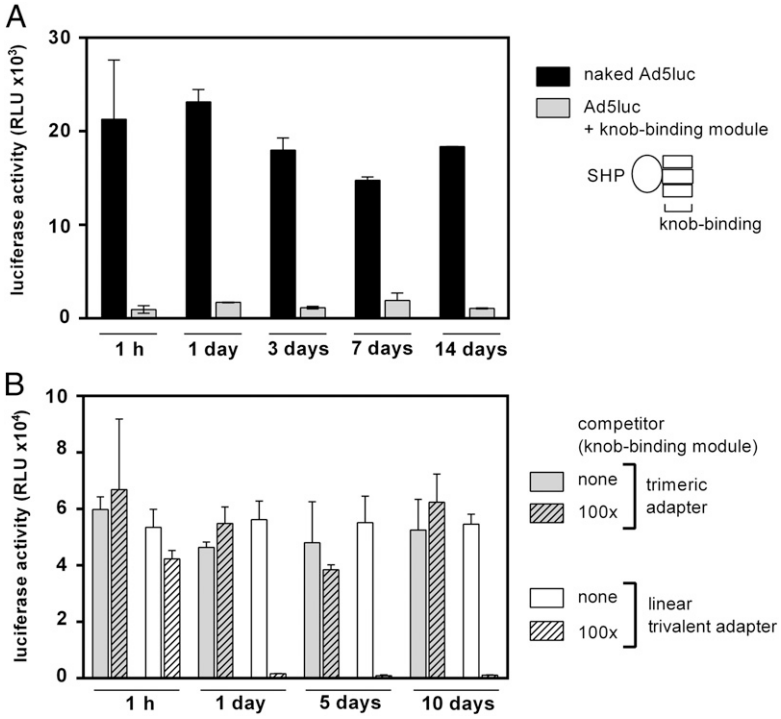

Fig. 5. Test of dissociation of DARPin-based adapters from the virus particle. (*A*) Integrity of infectivity of the virus itself and the bound knob-binding modules. Black bars represent infection with Ad5luc virus alone; gray bars represent infection with virus coated with 1D3nc_SHP1 (without the HER2-binding module) at an adapter:knob ratio of 1:1. Samples were incubated in PBS at room temperature for the time points indicated before infection of BT474 cells at 100 vp per cell. RLU were determined 16 h after infection. (*B*) Measurements of adapter dissociation from virus. Trimeric G3_1D3nc_SHP1 adapters (gray bars) or linear trivalent $(2E6)_3$_G5 adapters (white bars), both containing three knob-binding DARPins and a HER2-binding DARPin (G3 or G5), were incubated with Ad5luc at a 1:1 ratio of adapter to knob at room temperature for 1.5 h in PBS before the addition of a 100-fold excess of competitor 1D3nc_SHP1 (with no HER2-binding module) (hatched bars) to prevent reassociation of dissociated adapter or no competitor (white bars) as control. Samples were incubated at room temperature for the time points indicated before infection of BT474 cells at 100 vp per cell. RLU were determined 16 h after infection. All assays were performed in duplicate; error bars show the SD.

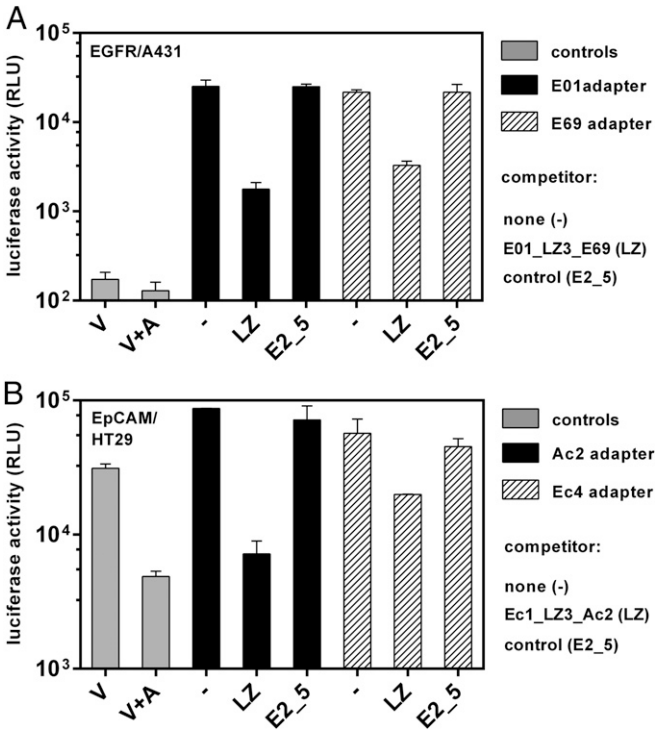

Fig. 6. Transduction of adapter-coated Ad5 using tumor cells overexpressing EGFR or EpCAM. (*A*) A431 cells were infected at a multiplicity of 100 vp per cell with a 1:1 ratio of trimeric adapter to knob. The trimeric 1D3nc_SHP1 knob-binding module was fused to either the EGFR-binding DARPin E01 (black bars) or E69 (hatched bars). Before infection the cells were incubated with 5 μM of the bispecific competitor E01_LZ3_E69 (LZ), a control DARPin E2_5, or no competitor (–). For controls (gray bars), cells were infected with virus alone (V) or with virus coated with 1D3nc_SHP1 (no EGFR-binding module) (V+A). (*B*) HT29 cells were infected at a multiplicity of 100 vp per cell with a 1:1 ratio of trimeric adapter to knob. The trimeric knob-binding module 1D3nc_SHP1 was fused to either the EpCAM-binding DARPin Ec4 (black bars) or Ac2 (striped bars). Before infection the cells were incubated with 5 μM of the bispecific competitor Ec1_LZ3_Ac2 (LZ), a control DARPin E2_5, or no competitor (–). For controls (gray bars), cells were infected with virus alone (V) or with virus coated with 1D3nc_SHP1 (with no EpCAM-binding module) (V+A). RLU were determined 16 h after infection. The assay was performed in duplicate; error bars show the SD.

observations suggest that even at the highest ratio of these linear adapters tested (100:1) some CAR-binding sites within the knobs remained unblocked by adapters, allowing the virus to bind to CAR expressed equally on both cell lines. In conclusion, these experiments clearly show the gains in the specificity by increased affinity of the adapter to the virion that resulted from the rational design of trimeric adapters made possible by the structural data generated earlier in the present study.

Trimeric Adapters Mediate Transduction of Tumor Cell Lines in an HER2-Dependent Manner. Because one possible application of the adapter strategy is its use in tumor targeting, it is essential to verify that various tumor cell lines can be transduced using a series of different tumor-associated surface receptors. As a first model system, we investigated the HER2-mediated transduction of adapter-coated Ad5luc using the HER2-overexpressing human breast tumor cell line BT474 (Fig. 4) (49). Transduction was achieved in an HER2-dependent manner when the DARPins G3 or 9.29 were fused to the knob-binding module, whereas only background luciferase activity was observed when the knob-binding module was fused to the control DARPin E2_5.

In contrast to the previous results using the HEK293 Flp-In cell line (Fig. 3*A*), which showed only moderate differences between the various adapter constructs, the differences were more dramatic using BT474 cells (Fig. 4). Whereas the C-terminal fusions of DARPin 9.29 showed transduction levels in the range of 40- to 57-fold above background (virus coated with the knob-binding module alone), G3 fusions were 49- to 102-fold over background, depending on the linker between the knob-binding DARPin 1D3nc and the SHP trimerization domain. For the N-terminal fusions the transduction levels of G3 were 107- to 231-fold over background, and the transduction levels of 9.29 were 164- to 293-fold over background. In conclusion, the N-terminal fusions showed much higher transduction levels than the C-terminal fusions. Furthermore, the most compact forms of the adapter (constructs containing SHP1 with a linker length of 1 aa or SHP2 with a linker length of 2 aa) as N-terminal fusions to the SHP trimerization domain seemed to be more efficient than SHP3 fusion proteins which contain an extended α-helix of 10 aa in the linker region between knob-binding DARPin 1D3nc and the SHP trimerization domain. Because the N-terminal fusion of the retargeting DARPin to the 1D3nc_SHP1 knob-binding module proved most efficient, it was used in all further experiments.

Trimeric Adapters Are Bound Stably to the Virus Particle with Very High Affinity. Next the stability of interaction of the trimeric adapter with the virus was compared with that of the linear adapters reported earlier, measured in terms of functional affinity (37). First, we needed to test whether the virus itself was stable at room temperature for the 2-wk duration of the experiment. Ad5luc alone incubated without adapter showed the same level of luciferase activity at all time points investigated, indicating that the virus was stable for up to 2 wk at room temperature (Fig. 5*A*). Second, the stability of the adapters and competitor was investigated. Therefore, the proteins either were incubated at room temperature for 2 wk or were freshly thawed and compared by SDS/PAGE (Fig. S11). The proteins showed no degradation during the course of the experiment. Third, and most importantly, the dissociation of the adapters from the virions was tested. For this purpose, the trimeric adapter G3_1D3nc_SHP1 or the linear trivalent adapter $(2E6)_3$_G5 was incubated with Ad5luc and subsequently incubated with a 100-fold excess of competitor (trimeric adapter without HER2-retargeting DARPin) for various time periods before transduction of BT474 cells (Fig. 5*B*). The purpose of the competitor was to prevent reassociation of the adapter, i.e., to make any dissociation event unidirectional and thus to elucidate the true off-rate. While the linear adapter $(2E6)_3$_G5 showed a reduction to background level after only 1 d of incubation with competitor, the trimeric adapter still conferred the same high transduction of BT474 cells after 10 d as observed initially in a HER2-dependent manner. To show the importance of the competitor in this experiment, we found that in its absence, after transduction of BT474 cells, the same signal intensity was observed for both adapters for all time points tested (Fig. 5*B*). This control showed that the reduction of luciferase is not a result of the deterioration of the linear trivalent adapter but due to its faster dissociation, i.e., lower functional affinity.

Together these results show that the trimeric adapters do not dissociate measurably over 10 d and therefore display a much higher functional affinity than the linear trivalent adapter.

Trimeric Adapters Can Be Constructed Readily with Different Targeting Specificities. To prove that the adapter strategy can be applied readily to other specificities, the HER2-binding module was replaced by modules recognizing other cell-surface receptors, such as EGFR and EpCAM. Adapters containing retargeting DARPins specific for EGFR or EpCAM were cloned, expressed, and purified. They were constructed in the adapter format 1D3nc_

SHP as N-terminal fusions, and their efficiency in transducing tumor cell lines overexpressing either EGFR or EpCAM was tested.

For Ad retargeting to EGFR, the DARPins E01 or E69 that bind to two distinct epitopes on EGFR (44, 50) were used. The specificity and efficiency of EGFR-mediated transduction was investigated using the previously described human epidermal carcinoma tumor cell line A431 overexpressing EGFR (Fig. 6*A*) (50). Ad5luc was coated with the adapters at an adapter-to-knob ratio of 1:1, and cells were infected at a multiplicity of 100 vp per cell. Both E01 and E69 adapters mediated transduction of A431 cells with an efficiency of 200-fold over virus alone (which represented the background level) (Fig. 6*A*). No transduction was observed for the EGFR-negative cell line CHO (Fig. S12*A*), suggesting that the EGFR-mediated transduction is indeed receptor specific. In addition, E01 adapter-coated Ad5luc infected CHO cells transiently expressing EGFR but not when EpCAM was overexpressed or the control CHO cells (Fig. S13*A*).

To show specificity of the transduction, a competition experiment was performed in which the cells were preincubated with a DARPin alone. When a bivalent and bispecific E69_E01 competitor, dimerized by a leucine zipper (LZ3) (50), was used, the transduction efficiency was reduced almost to background level both for the E01 adapter (to 7.2%) and for the E69 adapter (to 13%). Using the control DARPin E2_5 for competition, no reduction of transduction efficiency was observed (Fig. 6*A*).

To investigate EpCAM-mediated gene-transfer, the DARPins Ec4 or Ac2 were used as retargeting DARPins. They previously had been reported to bind EpCAM specifically at different epitopes (51). Adapters containing either retargeting module were used to coat Ad5luc at an adapter-to-knob ratio of 1:1 and their transduction efficiency was investigated (Fig. 6*B*). Both adapters mediated infection of the previously described EpCAM-overexpressing human colorectal adenocarcinoma cell line HT29 (51) (for Ac2, 18-fold over background, for Ec4, 12-fold over background). The transduction was receptor specific, because no luciferase was detected using the control cell line HEK293T expressing no EpCAM (Fig. S12*B*). In addition, the Ac2 and Ec4 adapter-coated Ad5luc infected CHO cells transiently expressing EpCAM, but not when EGFR was overexpressed or when CHO cells were used as control (Fig. S13*B*).

Competition experiments were performed to investigate further the specificity of the EpCAM adapters. The signals obtained were reduced only slightly, with no statistical significance, when the cells were preincubated with the control DARPin E2_5. In contrast, when the bispecific competitor Ec1_ Ac2 was used [Ec1 binds to the same epitope as Ec4 (51)], dimerized by LZ3, transduction efficiency was reduced to 1.5% for the Ac2 adapter and to 33% for the Ec4 adapter, demonstrating the specificity of transduction (Fig. 6*B*).

In conclusion, the retargeting module of the adapter can be exchanged readily to target different cell-surface receptors, validating the generic application of the trimeric knob-binding adapter strategy.

Discussion

Here, we describe an approach using DARPins toward a generic, universal system for efficient retargeting of Ad5 to a cell population of interest using an adapter strategy. While a genetic fusion of retargeting proteins to Ad capsid proteins would require the new construction and production of virus for every new epitope targeted and every new payload, an adapter-based strategy allows the use of generic, premade Ads containing a certain payload. An adapter strategy also can be used with nonpeptidic ligands (52). To date such approaches have been hampered by the low affinity of the adapter to the virus, leading to loss of specific interaction over time; also, when the virus construct retained intrinsic binding to virus receptors (e.g., CAR), unspecific virus entry to any CAR-expressing cells would result (24, 27–35).

We previously reported the selection of knob-binding DARPins to the fiber knob domain which were able to bind to both the WT and the knob domain mutated in the TAYT motif ablating CAR binding (37, 39). These monovalent DARPins bound at an affinity in the low nanomolar range (1.35 nM for 2E6) as determined by surface plasmon resonance (SPR), already better than approaches using the soluble CAR D1 domain displaying an affinity of only 15 nM (53). Trimerization of CAR D1-based adapters had been achieved using either the phage T4 fibritin domain or an isoleucine GCN4 trimerization domain (54, 55), which increased the efficiency of retargeting, but to our knowledge affinities have not been reported. The greatest obstacle in using these adapters was that they could be used only with WT Ad5, thus maintaining its intrinsic binding to CAR. Our approach aimed at generating trimeric adapters that could bind to Ad5 ablated in CAR binding. By linear multimerization we had previously achieved a functional affinity of better than 100 pM, but biophysical measurements suggested that only two DARPins might bind tightly per knob, with the third binding more weakly (37).

The crystal structure of the knob-binding DARPin 1D3 in complex with the trimeric knob protein allowed us to determine that the stoichiometry was clearly defined as three DARPins binding to one trimeric knob (Fig. 1), even though the B-factor (a measure of thermal motion) was much higher for one of the DARPins than for the other two. In solution, all three DARPins of the complex probably would show equal thermal mobilities, similar to the B-factor of chain F. This finding was a clear indication that, if ideally arranged on the knob, three DARPins could be positioned with greatly increased functional affinity. Moreover, the determination of the arrangement of the DARPins around the knob by X-ray crystallography suggested a better strategy than wrapping the DARPins around the knob linearly. Because the C termini are exposed at the top, we could fuse a highly stable trimeric protein, the capsid-stabilizing protein SHP of lambdoid phage 21 (43), allowing the DARPins to "clamp" the knob (Fig. 2 and Fig. S4). This adapter arrangement binds to the knob virtually irreversibly over 10 d, whereas the linear trimeric versions show measurable dissociation (Figs. 3 and 5*B*). This design thus is a great advance over other existing adapter-based approaches (24, 27–35, 37, 56).

DARPins are the ideal scaffold for large-scale production of such adapters (46, 57), because the absence of disulfides allows efficient soluble expression of these adapters with their multiple domains in the *E. coli* cytoplasm at very high levels (50–100 mg/mL) of culture. They spontaneously form very clean trimers after expression (Figs. S5 and S6). These properties make a scale-up for therapeutic products very realistic.

We have shown here that the knob-binding module, consisting of a knob-binding DARPin and the trimerization domain SHP, can be fused readily to a cell-surface receptor-binding DARPin, which will retarget Ad5 to a cell population expressing the respective cell-surface receptor (Figs. 3, 4, and 6). Because we can generate such retargeting DARPin modules to essentially any target using ribosome or phage display (37, 44, 50, 51, 58–64), we can exploit these capabilities [e.g., in tumor therapy in animal models (63, 65–67)] to use Ad5 to deliver payloads with tumor-controlling potential.

Although the performance of our trimeric bispecific adapters presented here still must be evaluated in vivo, it is clear that they have greatly improved properties—such as very high functional affinity, convenient exchange of the retargeting module, and high-level production—that represent major advances over the previously described adapter approaches.

Future studies will elucidate the efficacy of the trimeric adapters in vivo in combination with Ads that are ablated in their interaction of cells mediated by the fiber, penton base, or hexon protein (14).

Targeted Ads to date proved inefficient in vivo, especially when delivered systemically, as would be of the greatest clinical relevance, because the fiber-mediated transduction is undermined by clearance of Ad virions by Kupffer cells and robust fiber-independent transduction of hepatocytes (14, 68). In particular, it has been shown that the high efficacy of hepatic transduction by systemically injected Ad is caused by the extensive coverage of the virus surface by blood coagulation factor X. In essence, factor X functions as a bispecific targeting adapter linking the Ad hexon capsid protein hexon to heparin sulfate-containing proteoglycans present on hepatocytes (69, 70). Simply blocking the hexon-binding sites for factor X has not proven sufficient and was outcompeted by the high excess of factor X in the blood (27). More promising might be modifications of the hexon by replacing all hypervariable regions (HVRs) with the HVRs of hexons of Ad serotypes that do not bind factor X (13, 71) or by replacing or deleting amino acids in HVR5 involved in factor X binding (13, 56). Undoubtedly, Ads will have to be modified in several surface features simultaneously, and the adapter strategy will be useful in rapidly determining the most effective ones.

Here we have demonstrated a versatile strategy for rapidly generating Ad adapters with various cell-surface receptor specificities that clamp the Ad knob and bind virtually irreversibly to the virion. This generic adapter-based approach represents a generically applicable method to redirect prefabricated Ads to any cell population of choice. Although Ad vectors still will need to be engineered to reduce nontarget cell uptake, we present in this study a generic contribution toward efficient retargeting in future clinical applications.

Materials and Methods

Cloning, Expression, and Purification of DARPins, Knob, and Adapters. The knob-binding DARPins 1D3 and 2E6 were equipped with a stabilized C-cap (41, 42) and cloned into the expression vector pDST72 (44), a derivative of pQE30, by a PCR-based strategy. To construct adapters, the C terminus of the knob-binding DARPins (omitting the last three residues of the DARPin, which were disordered in the crystal structure) were fused to the N terminus of the phage capsid protein SHP, used as trimerization domain (43) (SHP, V13-P115), and was spaced by different linkers (SHP1, G; SHP2, GA; SHP3, GLKAGADVNA), introduced by a PCR-based strategy and cloned into pDST72. In a second step, the cDNA was inserted into pQIBi2_2 with either an N- or C-terminal fusion of the retargeting DARPins G3, 9.29, Ec4, Ac2, E01, or E69, reported earlier (44, 45, 50, 51), spaced by a $(Gly_4Ser)_4$ linker. These retargeting DARPins can be exchanged readily using either BamHI/HindIII (for N-terminal fusions) or BglII/BsaI (for C-terminal fusions). For competition, monomeric DARPins or bispecific DARPins with increased valency (LZ constructs) expressed and purified as previously described (37, 50, 51) were used. Expression of the $MA(H)_6$ mutant knobΔTAYT was performed as previously described (37).

Purification of DARPins, knob, and adapters was performed using immobilized-metal affinity chromatography (Ni-NTA superflow; QIAGEN) as previously described (37, 50, 51). Additional purification using SEC was performed in some cases using a Superdex 200 16/60 column (GE Healthcare Biosciences) in PBS (137 mM NaCl, 2.7 mM KCl, 10 mM Na_2HPO_4, 2 mM KH_2PO_4, pH 7.4) at a flow rate of 1 mL/min. For cloning, expression, purification, and refolding of the human CAR D1 domain see *SI Materials and Methods*.

Crystallization of the Knob-DARPin Complex. A first dataset was recorded in-house (MAR345 detector, Bruker Micro Star X-ray generator, Software GO 3.4.5.) at 2.7-Å resolution. A second dataset was recorded at the Swiss Light Source (Paul Scherrer Institute, Villagen, Switzerland) with a resolution of 1.95 Å, which was used for the refinement of the in-house–determined structure. The crystallization procedure is described in detail in *SI Materials and Methods*.

Cell Lines. Cell lines stably overexpressing HER2 were established using the HEK293 Flp-In or CHO Flp-In cell line (Invitrogen Ltd). Both were generated using the plasmid pcDNA5/FRT (Invitrogen Ltd.) into which the cDNA for HER2 (Gene Service) was inserted by a PCR-based strategy. Cells were transfected with Lipofectamine 2000 (Invitrogen Ltd.), and stable integrants were selected using hygromycin at a concentration of 150 μg/mL for HEK cells and 800 μg/mL for CHO cells. The HER2-overexpressing human breast ductal carcinoma tumor cell line BT474 (HTB-20), the EGFR-overexpressing human epidermal carcinoma cell line A431 (CRL-1555), the EpCAM-overexpressing human colorectal adenocarcinoma line HT29 (HTB-38), and the human epithelial embryonic kidney cell line HEK293T (CRL-1573) were all obtained from American Type Culture Collection. Cells generally were grown in DMEM (Ham's F-12 for CHO), 10% (vol/vol) FCS, penicillin/streptomycin, at 37 °C and 5% (vol/vol) CO_2.

Virus Production. A dual reporter based on an Ad5 expression system [kind gift of T. Trueb, University of Zurich (72, 73)] expressing both firefly luciferase and eGFP was cloned. After introduction of the bicistronic construct spaced by an internal ribosome entry site sequence into the transfer vector pCTA, Cre-mediated recombination was performed in the *E. coli* strain Bm28.5 for integration of the expression cassette into the viral genome (pAdlox). The recombinant adenoviral DNA was used to transfect the complementing cell line HEK293 WT using Lipofectamine 2000 (Invitrogen Ltd.). Recombinant virus was amplified over several rounds of infection. For purification of virus 30 × 15 cm plates were harvested and processed as previously described using a CsCl gradient (74). Virus concentration was determined using OD_{260} with a conversion factor of 9.09×10^{13} vp per absorbance unit at 260 nm (75).

Transduction Experiments. If not otherwise stated, transduction experiments were performed in a 24-well format with 2×10^5 cells per well using a multiplicity of 100 vp per cell. Recombinant virus was incubated with a 1:1 ratio of adapter per knob for 1 h at room temperature. Cells were infected and incubated at 37 °C, 5% (vol/vol) CO_2 for 1 h. The medium was replaced, and cells were incubated further for 14–18 h as indicated. For analysis of luciferase activity the medium was removed, cells were lysed in 300 μL cell lysis buffer, and activity was determined using luciferase reporter assay solution (Promega) and a Victor3 plate luminometer (PerkinElmer Inc.). For competition studies testing specificity, the cells were preincubated with competitor protein for 1–1.5 h before transduction. For competition studies investigating the stability of the adapter, adapter and virus were mixed and incubated for 1.5 h before a 100-fold excess of competitor was added and incubated for different lengths of time before infection.

ACKNOWLEDGMENTS. We thank Beat Blattmann and Céline Stutz-Ducommun from the in-house National Centers of Competence in Research (NCCR) crystallization unit for their assistance during the crystallization process; Nikolas Stefan and Manuel Simon for sharing epithelial cell adhesion molecule-related reagents; Ykelien Boersma for epidermal growth factor receptor-related reagents; Philipp Schätzle for his introduction to adenovirus generation and production; and Simon Hansen for help in surface plasmon resonance evaluation. This work was funded by a grant from the NCCR Structural Biology to A.P., by European Research Council senior investigator Grant NEXTBINDERS 268621 (to A.P.), by the University of Zurich, and Grants R01 CA128807, R01 CA116621, and R21 EB012259 from the National Institutes of Health.

1. Amalfitano A, Parks RJ (2002) Separating fact from fiction: Assessing the potential of modified adenovirus vectors for use in human gene therapy. *Curr Gene Ther* 2(2): 111–133.
2. Edelstein ML, Abedi MR, Wixon J (2007) Gene therapy clinical trials worldwide to 2007—an update. *J Gene Med* 9(10):833–842.
3. Verma IM, Weitzman MD (2005) Gene therapy: Twenty-first century medicine. *Annu Rev Biochem* 74:711–738.
4. Bergelson JM, et al. (1997) Isolation of a common receptor for Coxsackie B viruses and adenoviruses 2 and 5. *Science* 275(5304):1320–1323.
5. Tomko RP, Xu R, Philipson L (1997) HCAR and MCAR: The human and mouse cellular receptors for subgroup C adenoviruses and group B coxsackieviruses. *Proc Natl Acad Sci USA* 94(7):3352–3356.
6. Arnberg N, Edlund K, Kidd AH, Wadell G (2000) Adenovirus type 37 uses sialic acid as a cellular receptor. *J Virol* 74(1):42–48.
7. Gaggar A, Shayakhmetov DM, Lieber A (2003) CD46 is a cellular receptor for group B adenoviruses. *Nat Med* 9(11):1408–1412.
8. Short JJ, et al. (2004) Adenovirus serotype 3 utilizes CD80 (B7.1) and CD86 (B7.2) as cellular attachment receptors. *Virology* 322(2):349–359.
9. Wang H, et al. (2011) Desmoglein 2 is a receptor for adenovirus serotypes 3, 7, 11 and 14. *Nat Med* 17(1):96–104.
10. Wickham TJ, Mathias P, Cheresh DA, Nemerow GR (1993) Integrins $\alpha_v\beta_3$ and $\alpha_v\beta_5$ promote adenovirus internalization but not virus attachment. *Cell* 73(2):309–319.
11. Nemerow GR, Pache L, Reddy V, Stewart PL (2009) Insights into adenovirus host cell interactions from structural studies. *Virology* 384(2):380–388.

12. Russell WC (2009) Adenoviruses: Update on structure and function. *J Gen Virol* 90(Pt 1):1–20.
13. Alba R, et al. (2009) Identification of coagulation factor (F)X binding sites on the adenovirus serotype 5 hexon: Effect of mutagenesis on FX interactions and gene transfer. *Blood* 114(5):965–971.
14. Khare R, Chen CY, Weaver EA, Barry MA (2011) Advances and future challenges in adenoviral vector pharmacology and targeting. *Curr Gene Ther* 11(4):241–258.
15. Koizumi N, et al. (2006) Modified adenoviral vectors ablated for coxsackievirus-adenovirus receptor, α_v integrin, and heparan sulfate binding reduce in vivo tissue transduction and toxicity. *Hum Gene Ther* 17(3):264–279.
16. Krasnykh VN, Douglas JT, van Beusechem VW (2000) Genetic targeting of adenoviral vectors. *Mol Ther* 1(5 Pt 1):391–405.
17. Nicklin SA, Wu E, Nemerow GR, Baker AH (2005) The influence of adenovirus fiber structure and function on vector development for gene therapy. *Mol Ther* 12(3): 384–393.
18. Noureddini SC, Curiel DT (2005) Genetic targeting strategies for adenovirus. *Mol Pharm* 2(5):341–347.
19. Coughlan L, et al. (2010) Tropism-modification strategies for targeted gene delivery using adenoviral vectors. *Viruses* 2(10):2290–2355.
20. Philipson L, Pettersson RF (2004) The coxsackie-adenovirus receptor—a new receptor in the immunoglobulin family involved in cell adhesion. *Curr Top Microbiol Immunol* 273:87–111.
21. Belousova N, et al. (2003) Genetically targeted adenovirus vector directed to CD40-expressing cells. *J Virol* 77(21):11367–11377.
22. Belousova N, Mikheeva G, Gelovani J, Krasnykh V (2008) Modification of adenovirus capsid with a designed protein ligand yields a gene vector targeted to a major molecular marker of cancer. *J Virol* 82(2):630–637.
23. Krasnykh VN, Mikheeva GV, Douglas JT, Curiel DT (1996) Generation of recombinant adenovirus vectors with modified fibers for altering viral tropism. *J Virol* 70(10): 6839–6846.
24. Wickham TJ, et al. (1997) Increased in vitro and in vivo gene transfer by adenovirus vectors containing chimeric fiber proteins. *J Virol* 71(11):8221–8229.
25. Magnusson MK, et al. (2012) A transductionally retargeted adenoviral vector for virotherapy of Her2/neu-expressing prostate cancer. *Hum Gene Ther* 23(1):70–82.
26. Waehler R, Russell SJ, Curiel DT (2007) Engineering targeted viral vectors for gene therapy. *Nat Rev Genet* 8(8):573–587.
27. Chen CY, May SM, Barry MA (2010) Targeting adenoviruses with factor x-single-chain antibody fusion proteins. *Hum Gene Ther* 21(6):739–749.
28. Dmitriev I, Kashentseva E, Rogers BE, Krasnykh V, Curiel DT (2000) Ectodomain of coxsackievirus and adenovirus receptor genetically fused to epidermal growth factor mediates adenovirus targeting to epidermal growth factor receptor-positive cells. *J Virol* 74(15):6875–6884.
29. Ebbinghaus C, et al. (2001) Functional and selective targeting of adenovirus to high-affinity Fcgamma receptor I-positive cells by using a bispecific hybrid adapter. *J Virol* 75(1):480–489.
30. Haisma HJ, et al. (2010) Selective targeting of adenovirus to $\alpha_v\beta_3$ integrins, VEGFR2 and Tie2 endothelial receptors by angio-adenobodies. *Int J Pharm* 391(1-2):155–161.
31. Hong SS, Galaup A, Peytavi R, Chazal N, Boulanger P (1999) Enhancement of adenovirus-mediated gene delivery by use of an oligopeptide with dual binding specificity. *Hum Gene Ther* 10(16):2577–2586.
32. Korokhov N, et al. (2003) Targeting of adenovirus via genetic modification of the viral capsid combined with a protein bridge. *J Virol* 77(24):12931–12940.
33. Pereboev AV, et al. (2004) Enhanced gene transfer to mouse dendritic cells using adenoviral vectors coated with a novel adapter molecule. *Mol Ther* 9(5):712–720.
34. Reynolds PN, et al. (2000) A targetable, injectable adenoviral vector for selective gene delivery to pulmonary endothelium in vivo. *Mol Ther* 2(6):562–578.
35. Watkins SJ, Mesyanzhinov VV, Kurochkina LP, Hawkins RE (1997) The 'adenobody' approach to viral targeting: Specific and enhanced adenoviral gene delivery. *Gene Ther* 4(10):1004–1012.
36. Wickham TJ, et al. (1996) Targeted adenovirus gene transfer to endothelial and smooth muscle cells by using bispecific antibodies. *J Virol* 70(10):6831–6838.
37. Dreier B, et al. (2011) Her2-specific multivalent adapters confer designed tropism to adenovirus for gene targeting. *J Mol Biol* 405(2):410–426.
38. Zlotnick A, Stray SJ (2003) How does your virus grow? Understanding and interfering with virus assembly. *Trends Biotechnol* 21(12):536–542.
39. Kirby I, et al. (1999) Mutations in the DG loop of adenovirus type 5 fiber knob protein abolish high-affinity binding to its cellular receptor CAR. *J Virol* 73(11):9508–9514.
40. Roelvink PW, Mi Lee G, Einfeld DA, Kovesdi I, Wickham TJ (1999) Identification of a conserved receptor-binding site on the fiber proteins of CAR-recognizing adenoviridae. *Science* 286(5444):1568–1571.
41. Wetzel SK, et al. (2010) Residue-resolved stability of full-consensus ankyrin repeat proteins probed by NMR. *J Mol Biol* 402(1):241–258.
42. Wetzel SK, Settanni G, Kenig M, Binz HK, Plückthun A (2008) Folding and unfolding mechanism of highly stable full-consensus ankyrin repeat proteins. *J Mol Biol* 376(1): 241–257.
43. Forrer P, Chang C, Ott D, Wlodawer A, Plückthun A (2004) Kinetic stability and crystal structure of the viral capsid protein SHP. *J Mol Biol* 344(1):179–193.
44. Steiner D, Forrer P, Plückthun A (2008) Efficient selection of DARPins with sub-nanomolar affinities using SRP phage display. *J Mol Biol* 382(5):1211–1227.
45. Zahnd C, et al. (2007) A designed ankyrin repeat protein evolved to picomolar affinity to Her2. *J Mol Biol* 369(4):1015–1028.
46. Binz HK, Stumpp MT, Forrer P, Amstutz P, Plückthun A (2003) Designing repeat proteins: Well-expressed, soluble and stable proteins from combinatorial libraries of consensus ankyrin repeat proteins. *J Mol Biol* 332(2):489–503.
47. Bewley MC, Springer K, Zhang YB, Freimuth P, Flanagan JM (1999) Structural analysis of the mechanism of adenovirus binding to its human cellular receptor, CAR. *Science* 286(5444):1579–1583.
48. Gensler M, Buschbeck M, Ullrich A (2004) Negative regulation of HER2 signaling by the PEST-type protein-tyrosine phosphatase BDP1. *J Biol Chem* 279(13):12110–12116.
49. Belousova N, et al. (2010) Development of a targeted gene vector platform based on simian adenovirus serotype 24. *J Virol* 84(19):10087–10101.
50. Boersma YL, Chao G, Steiner D, Wittrup KD, Plückthun A (2011) Bispecific designed ankyrin repeat proteins (DARPins) targeting epidermal growth factor receptor inhibit A431 cell proliferation and receptor recycling. *J Biol Chem* 286(48):41273–41285.
51. Stefan N, et al. (2011) DARPins recognizing the tumor-associated antigen EpCAM selected by phage and ribosome display and engineered for multivalency. *J Mol Biol* 413(4):826–843.
52. Simon M, Zangemeister-Wittke U, Plückthun A (2012) Facile double-functionalization of designed ankyrin repeat proteins using click and thiol chemistries. *Bioconjug Chem* 23(2):279–286.
53. Kirby I, et al. (2000) Identification of contact residues and definition of the CAR-binding site of adenovirus type 5 fiber protein. *J Virol* 74(6):2804–2813.
54. Kashentseva EA, Seki T, Curiel DT, Dmitriev IP (2002) Adenovirus targeting to c-erbB-2 oncoprotein by single-chain antibody fused to trimeric form of adenovirus receptor ectodomain. *Cancer Res* 62(2):609–616.
55. Kim J, et al. (2002) Targeting adenoviral vectors by using the extracellular domain of the coxsackie-adenovirus receptor: Improved potency via trimerization. *J Virol* 76(4): 1892–1903.
56. Alba R, et al. (2010) Biodistribution and retargeting of FX-binding ablated adenovirus serotype 5 vectors. *Blood* 116(15):2656–2664.
57. Binz HK, et al. (2004) High-affinity binders selected from designed ankyrin repeat protein libraries. *Nat Biotechnol* 22(5):575–582.
58. Boersma YL, Plückthun A (2011) DARPins and other repeat protein scaffolds: Advances in engineering and applications. *Curr Opin Biotechnol* 22(6):849–857.
59. Dreier B, Plückthun A (2012) Rapid selection of high-affinity binders using ribosome display. *Methods Mol Biol* 805:261–286.
60. Hanes J, Jermutus L, Weber-Bornhauser S, Bosshard HR, Plückthun A (1998) Ribosome display efficiently selects and evolves high-affinity antibodies in vitro from immune libraries. *Proc Natl Acad Sci USA* 95(24):14130–14135.
61. Hanes J, Plückthun A (1997) In vitro selection and evolution of functional proteins by using ribosome display. *Proc Natl Acad Sci USA* 94(10):4937–4942.
62. Plückthun A (2012) Ribosome display: A perspective. *Methods Mol Biol* 805:3–28.
63. Tamaskovic R, Simon M, Stefan N, Schwill M, Plückthun A (2012) Designed ankyrin repeat proteins (DARPins) from research to therapy. *Methods Enzymol* 503:101–134.
64. Zahnd C, Amstutz P, Plückthun A (2007) Ribosome display: Selecting and evolving proteins in vitro that specifically bind to a target. *Nat Methods* 4(3):269–279.
65. Martin-Killias P, Stefan N, Rothschild S, Plückthun A, Zangemeister-Wittke U (2011) A novel fusion toxin derived from an EpCAM-specific designed ankyrin repeat protein has potent antitumor activity. *Clin Cancer Res* 17(1):100–110.
66. Theurillat JP, et al. (2010) Designed ankyrin repeat proteins: A novel tool for testing epidermal growth factor receptor 2 expression in breast cancer. *Mod Pathol* 23(9): 1289–1297.
67. Zahnd C, et al. (2010) Efficient tumor targeting with high-affinity designed ankyrin repeat proteins: Effects of affinity and molecular size. *Cancer Res* 70(4):1595–1605.
68. Xu Z, Tian J, Smith JS, Byrnes AP (2008) Clearance of adenovirus by Kupffer cells is mediated by scavenger receptors, natural antibodies, and complement. *J Virol* 82(23): 11705–11713.
69. Kalyuzhniy O, et al. (2008) Adenovirus serotype 5 hexon is critical for virus infection of hepatocytes in vivo. *Proc Natl Acad Sci USA* 105(14):5483–5488.
70. Waddington SN, et al. (2008) Adenovirus serotype 5 hexon mediates liver gene transfer. *Cell* 132(3):397–409.
71. Roberts DM, et al. (2006) Hexon-chimaeric adenovirus serotype 5 vectors circumvent pre-existing anti-vector immunity. *Nature* 441(7090):239–243.
72. Chartier C, et al. (1996) Efficient generation of recombinant adenovirus vectors by homologous recombination in *Escherichia coli*. *J Virol* 70(7):4805–4810.
73. Mohanty S, et al. (2005) Overexpression of IRS2 in isolated pancreatic islets causes proliferation and protects human beta-cells from hyperglycemia-induced apoptosis. *Exp Cell Res* 303(1):68–78.
74. Becker TC, et al. (1994) Use of recombinant adenovirus for metabolic engineering of mammalian cells. *Methods Cell Biol* 43(Pt A):161–189.
75. Mittereder N, March KL, Trapnell BC (1996) Evaluation of the concentration and bioactivity of adenovirus vectors for gene therapy. *J Virol* 70(11):7498–7509.

Supporting Information

Dreier et al. 10.1073/pnas.1213653110

SI Materials and Methods

Crystallization of the Knob-DARPin Complex. Immobilized-metal affinity chromatography–purified designed ankyrin repeat protein (DARPin) 1D3 was mixed with MA(H)$_6$ knobΔTAYT in a molar ratio of 1 subunit to 1.5 DARPins and incubated for 2 h on ice for complex formation. The complex was purified by size-exclusion chromatography (SEC) (Superdex 200 16/60, PBS at pH 7.4, 1 mL/min) and concentrated using Amicon-Ultra concentrators (Millipore) with a molecular weight cutoff of 10 kDa. Crystals grew in 0.1 M citric acid, 5% polyethylene glycol (PEG) 6000 (vol/vol) at pH 5. For refinement a screen with a pH gradient on the *x* axis (ranging from pH 4 to pH 7) and a PEG 400 gradient (ranging from 0 to 20% vol/vol) on the *y* axis was performed. A dataset of a crystal grown at 8.95 mg/mL protein in 0.1 M citric acid, 2.86% (vol/vol) PEG 400 at pH 5.36 was recorded in-house (MAR345 detector, Bruker Micro Star X-ray generator, Software GO 3.4.5.). Twenty percent ethylene glycol in 0.1 M citric acid was determined to be the best cryoprotectant. The best resolution that could be obtained was 2.7 Å. A second dataset recorded at the Swiss Light Source (Paul Scherrer Institute, Villigen, Switzerland) with a resolution of 1.95 Å was used for the refinement of the in-house determined structure.

The data were processed with X-ray Detector Software XDS (1, 2), and the primitive orthorhombic space group $P2_12_12_1$ was determined. Molecular replacement using the programs PHASER (3) and MOLREP (4), which are part of the CCP4 program suite, was performed using the structure of WT knob [Protein Data Bank (PDB) ID 1knb (5)] as well as a structure of a consensus DARPin (PDB ID 2qyj) (6) as a search model. The complex had a three DARPin to three knob subunit stoichiometry in the space group $P2_12_12_1$ in the asymmetric unit. The refinement was performed using REFMAC 5.2.0019 (7) and PHENIX (8). The initial refinement steps were done by rigid body refinement followed by restrained refinement with isotropic B-factors. The completely refined structure revealed a working R-factor of 19.4% and a free R-factor of 22.16% for 110,875 unique reflections. The refined atomic model contains 691 water molecules. The first 19 residues of the knob as well as the first 12 residues (containing a His$_6$ tag) and the terminal three residues of the DARPin could not be modeled because of lack of electron density. The statistics of data collection and the refinement are given in Table S1.

Surface Plasmon Resonance. Surface plasmon resonance (SPR) experiments were performed using a BIAcore 3000 system (GE Healthcare Biosciences). Biotinylated MA(H)$_6$ knobΔTAYT protein was immobilized on a BIAcore streptavidin-coated sensor chip at 150 response units (RU). Measurements were performed at 25 °C in HBST buffer (20 mM Hepes, 150 mM NaCl, 3 mM EDTA, and 0.005% Tween-20). Injection was performed for 5 min at a flow rate of 30 μL/min followed by a dissociation time of 40 or 60 min depending on the experiment. The data were analyzed using Scrubber2 (Myszka and collaborators; BioLogic Software) in combination with CLAMP XP version 3.5 (developed by the Center for Biomolecular Interaction Analysis at the University of Utah, www.cores.utah.edu/interaction) to determine the affinity of the proteins.

SEC Coupled to Multiangle Light Scattering. The mass, biophysical properties, and oligomeric state of the trimeric knob-binding modules were analyzed using SEC (LC1100 System; Agilent Technologies) coupled to an Optilab rEX refractometer (Wyatt Technology) and a miniDAWN three-angle light-scattering detector (Wyatt Technology). For protein separation, a 24-mL Superdex 200 10/30 column (GE Healthcare Biosciences) was run at 0.5 mL/min in PBS (137 mM NaCl, 2.7 mM KCl, 10 mM Na_2HPO_4, 2 mM KH_2PO_4, pH 7.4). To determine the stoichiometry of the DARPin 1D3nc_SHP/knob complex 50 μL of a protein solution was injected. Data analysis was carried out with the ASTRA software (version 5.2.3.15; Wyatt Technology).

ELISA. Briefly, to investigate simultaneous binding of human epidermal growth factor receptor 2 (HER2) and knob to the DARPin adapters, ELISA was performed using 100 μL of 25 nM HER2 extracellular domains (ECD) 1–4 (kind gift of T. Adams, Commonwealth Scientific and Industrial Research Organisation, Parkville VIC, Australia) for immobilization on a Maxisorp 96-well plate (Nunc) for 1 h at room temperature. After unbound target was removed with two washes of PBS containing 0.05% Tween 20 (PBST), the wells were blocked with 0.5% BSA in PBST for 1 h at room temperature. Then 100 μL of 33 nM trimeric DARPin adapters was incubated for 1 h at room temperature, and unbound DARPins was removed with two washes of PBST. Knob protein that was biotinylated at an AviTag (Avidity) was incubated at a concentration of 100 nM before detection using a streptavidin-AP conjugate (11093266910; Roche) at a 1:5,000 dilution.

To investigate exclusive binding of Coxsackievirus-and-Ad receptor (CAR) or knob-binding DARPin, the recombinant biotinylated trimeric WT knob protein was immobilized at a concentration of 10 nM to wells of a NeutrAvidin-coated Maxisorp 96-well plate (Nunc) for 1 h at room temperature. Unbound knob then was removed with two washes of PBST, and wells were blocked with 0.5% BSA in PBST for 1 h at room temperature. The refolded, purified human CAR D1 domain fused to an HA tag at a concentration of 30 nM, and various knob-binding DARPin formats at a concentration of 100 nM were mixed. One hundred microliters of the CAR-DARPin mixtures was added and incubated at room temperature for 1 h. After washing with PBST, detection of the bound CAR D1 domain was performed using a mouse anti-HA antibody (Sigma-Aldrich Corp.) (dilution of 1:10,000), followed by a secondary goat anti-mouse antibody coupled to alkaline phosphatase (Sigma-Aldrich Corp) (dilution of 1:10,000).

For ELISA-based assays p-nitrophenyl phosphate (1:300 dilution of a 1-M stock) was used as substrate, and signals were measured at an absorbance of 405 nm.

Expression, Purification, and Refolding of the Human CAR D1 Domain. The human CAR D1 domain was amplified using PCR from an IMAGE clone in pCMVSport6 (NIH_MGC_12; Gene Service) and cloned into the expression plasmid pET28a(+) (Novagen). After sequence verification the protein was expressed by the addition of 1 mM isopropylthio-β-galactoside in BL21(DE3) with an N-terminal fusion to a His$_6$ tag for purification and C-terminal fusion to a HA tag for detection. The CAR D1 domain formed inclusion bodies. Therefore, cells were lysed by sonication, and inclusion bodies were prepared by three washes with PBS/Triton X-100 and sonication. Solubilization of inclusion bodies was performed in 100 mM Tris, 6 M guanidine hydrochloride (GdnHCl) (pH 7.3), 4 mM DTT. The CAR D1 domain was purified over a Ni-NTA column (QIAGEN) under denaturing conditions using 6 M GdnHCl. Elution was performed in 100 mM NaH_2PO_4, 10 mM Tris, 8 M urea at pH 4.5. The protein was refolded

in 100 mM Tris (pH 7.5), 100 mM NaCl, 3 mM glutathione, and 0.3 mM glutathione disulfide. The sample was dialyzed against PBS.

Transient Transfection of CHO Flp-in Cells. CHO Flp-In cells (Invitrogen) were transiently transfected at 90% confluency with 1 μg plasmid DNA and 2 μL Lipofectamine 2000 (Invitrogen) per well of a 24-well plate. Twenty-four hours after transfection the medium was replaced, and cells were allowed to grow for another 6 h at 37 °C, 5% (vol/vol) CO_2 before infection with adapter-coated Ad5luc. Plasmids used for transient transfection were pcDNA3.1(+)_HER2 (subcloned from pENTR223.1 hErbB2, NIH MGC 428; Geneservice), pBabePuro_EGFRwt (Addgene plasmid 11011) (9), and pcDNA5/FRT_EpCAM (subcloned from cDNA published in ref. 10).

1. Kabsch W (1988) Evaluation of single-crystal X-ray diffraction data from a position-sensitive detector. *J Appl Cryst* 21(6):916–924.
2. Kabsch W (1993) Automatic processing of rotation diffraction data from crystals of initially unknown symmetry and cell constants. *J Appl Cryst* 26(6):795–800.
3. McCoy AJ, et al. (2007) Phaser crystallographic software. *J Appl Cryst* 40(Pt 4):658–674.
4. Vagin AT, Teplyakov A (1997) MOLREP: An automated program for molecular replacement. *J Appl Cryst* 30(6):1022–1025.
5. Xia D, Henry LJ, Gerard RD, Deisenhofer J (1994) Crystal structure of the receptor-binding domain of adenovirus type 5 fiber protein at 1.7 A resolution. *Structure* 2(12): 1259–1270.
6. Merz T, et al. (2008) Stabilizing ionic interactions in a full-consensus ankyrin repeat protein. *J Mol Biol* 376(1):232–240.
7. Murshudov GN, Vagin AA, Dodson EJ (1997) Refinement of macromolecular structures by the maximum-likelihood method. *Acta Crystallogr D Biol Crystallogr* 53(Pt 3):240–255.
8. Adams PD, et al. (2002) PHENIX: Building new software for automated crystallographic structure determination. *Acta Crystallogr D Biol Crystallogr* 58(Pt 11):1948–1954.
9. Greulich H, et al. (2005) Oncogenic transformation by inhibitor-sensitive and -resistant EGFR mutants. *PLoS Med* 2(11):e313.
10. Münz M, et al. (2004) The carcinoma-associated antigen EpCAM upregulates c-myc and induces cell proliferation. *Oncogene* 23(34):5748–5758.

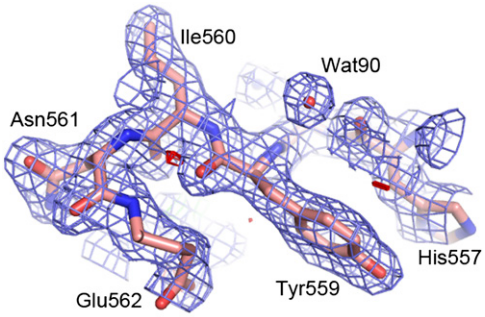

Fig. S1. Electron density at the Ad5 knob/1D3 interface. Depicted are the interface residues His557 to Glu562 of the knob chain A, the 3Fo-2Fc electron density map (dark blue, contour level 1.2 σ).

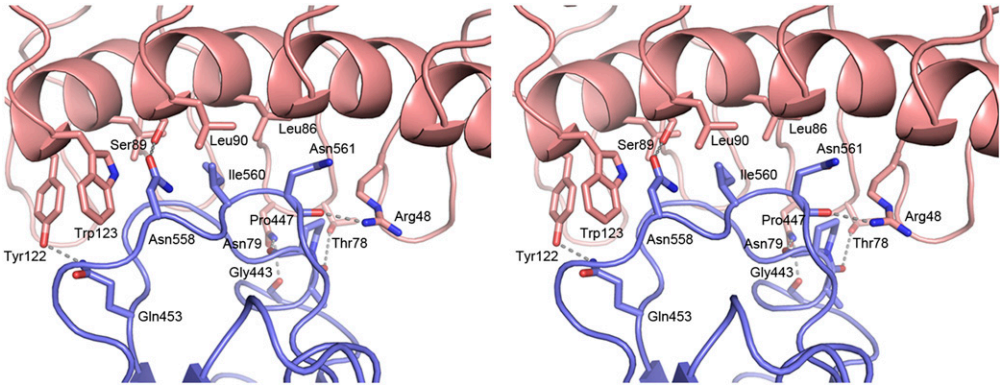

Fig. S2. Close-up view of the Ad5 knob/1D3 interface. TheAd5 knob is represented by the blue ribbon; DARPin 1D3 is represented by the salmon ribbon. Each 1D3 DARPin recognizes one subunit of the Ad5 knob trimer with an interface area of 690 ± 19 $Å^2$. This interaction is formed between the randomized positions of all three internal DARPin repeats and the surface-exposed loops of the Ad5 knob, involving residues 443–451 and 558–563. The interface involves several hydrogen bonds and van der Waals contacts. In particular, Ile560 from the Ad5 knob fits nicely into a hydrophobic pocket formed by Leu86, Leu90, and Leu119 from 1D3. In addition to five short intermolecular hydrogen bonds, the side chain of Thr78 forms a stretched hydrogen bond with the main chain carbonyl oxygen of Ala446. This interaction is remarkable, because Ala446 forms a *cis*-peptide bond with Pro447, and thus the DARPin uses a rather rare feature as part of the recognition surface.

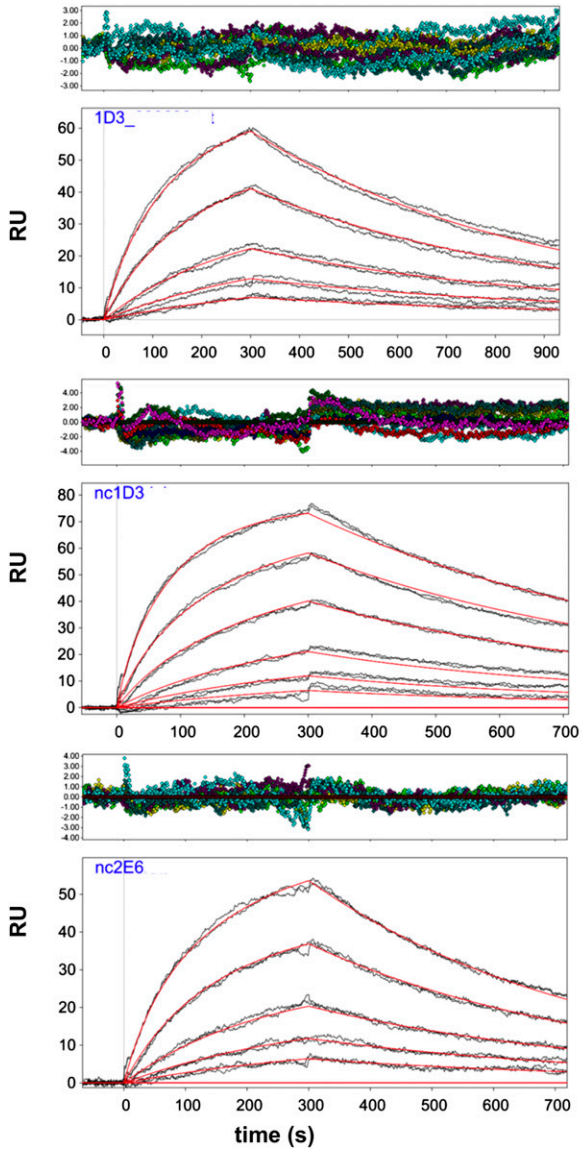

DARPin 1D3				
Association ($\times 10^6\ M^{-1}\ s^{-1}$)		Dissociation ($\times 10^{-3}\ s^{-1}$)		K_D
k_{a1}	2.7	k_{d1}	0.673	0.25 ± 0.02 nM
k_{a2}	0.463	k_{d2}	1.805	3.9 ± 0.14 nM

DARPin 1D3nc				
Association ($\times 10^6\ M^{-1}\ s^{-1}$)		Dissociation ($\times 10^{-3}\ s^{-1}$)		K_D
k_{a1}	1.47	k_{d1}	1.11	0.753 ± 0.01 nM
k_{a2}	0.239	k_{d2}	1.9	7.94 ± 0.22 nM

DARPin 2E6nc				
Association ($\times 10^6\ M^{-1}\ s^{-1}$)		Dissociation ($\times 10^{-3}\ s^{-1}$)		K_D
k_{a1}	2.09	k_{d1}	1.54	0.735 ± 0.02 nM
k_{a2}	0.275	k_{d2}	1.242	8.79 ± 0.59 nM

Fig. S3. Affinity of knob-binding DARPins. SPR experiments were performed using immobilized knob protein and different concentrations of DARPins 1D3, 1D3nc, and 2E6nc. Measurements were performed in duplicate at concentrations of 20, 10, 5, 2, 1, and 0.5 nM for 1D3nc and at concentrations of 10, 5, 2, 1, and 0.5 nM for 1D3 and 2E6nc. From the resulting binding curves (*Left*) the affinity of the proteins was determined using a heterogeneous ligand model (*Right*). The heterogeneous ligand model is consistent with the crystal structure in which the interface with the three bound DARPins is not identical. RU were plotted against time (in s). The residuals are displayed at the top of the corresponding graph. Black curves represent duplicate measurements; the red curves show the respective fit.

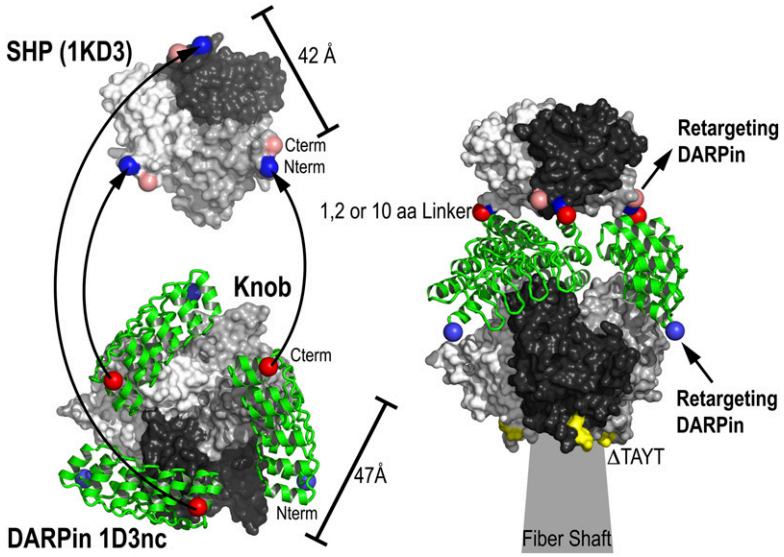

Fig. S4. Rational design of a trimeric clamp using the SHP trimerization motif. (*Left*) Top view, open sandwich representation. (*Right*) Side view of a model of the assembled structure. The last three amino acids of the DARPin in the structure of the DARPin-knob complex and the first 12 amino acids in the structure of the SHP trimer (PDB ID 1KD3) (1) are not resolved. The N-terminal amino groups of the three SHP subunits visible in the trimer (blue spheres) are 40.3, 42.6, and 42.8 Å apart. The C termini of the DARPins (red spheres) in the knob-DARPin complex are 46.5, 48.1, and 47.7 Å apart. In the top view, the curved arrows indicate where a short connecting linker has been introduced between the C terminus of the DARPin and the N terminus of SHP. Three versions were constructed with the following amino acids: SHP1, G; SHP2, GA; and SHP3, GLKAGADVNA. In the side view, the arrows (direction following the peptide chain) indicate two different attachments of a flexible linker at the end of which a retargeting DARPin was fused. The four amino acids surrounding the ΔTAYT deletion abolishing CAR-binding are colored in yellow.

1. Forrer P, Chang C, Ott D, Wlodawer A, Plückthun A (2004) Kinetic stability and crystal structure of the viral capsid protein SHP. *J Mol Biol* 344(1):179–193.

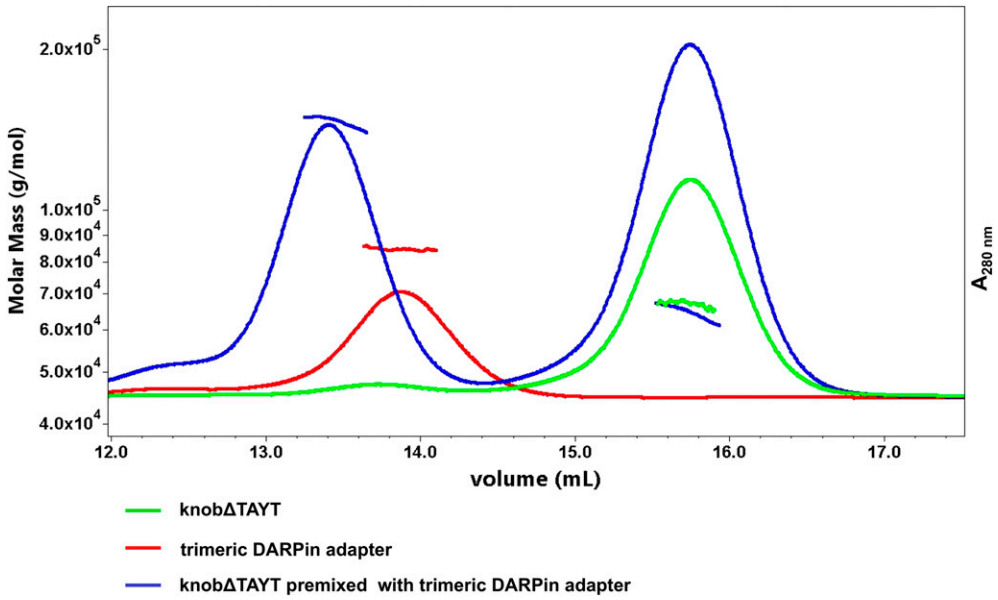

Fig. S5. Trimerization of the knob-binding DARPin 1D3nc. The knob-binding DARPin 1D3nc with stabilized C-cap (1, 2) was fused to the N terminus of the trimerization domain SHP (3) spaced by different linkers (compare Fig. 2 in the main text and Fig. S4). Their mass, biophysical properties, and oligomeric state were analyzed using SEC-multiangle light scattering (MALS). Fifty microliters of a solution containing 60 μM trimeric $A(H)_6$ knobΔTAYT protein alone (green line; expected molar mass, 66 kDa) or 30 μM of the trimeric DARPin knob-binding module (red line; expected molar mass for the trimer containing SHP1, 85 kDa) was injected. To investigate the stoichiometry of complex formation knob and DARPin SHP fusions were mixed and incubated for 1 h at 4 °C before injection. For clarity only the result for 1D3nc_SHP1 is shown, for which a molar mass of 84.5 kDa corresponding to the trimer was determined. All knob-binding 1D3nc_SHP fusions formed trimers and showed a clear 1:1 stoichiometry (blue line; complex and free knob) as determined by the molar mass of the complex at 146 kDa (expected molar mass of the complex, 151 kDa).

1. Wetzel SK, et al. (2010) Residue-resolved stability of full-consensus ankyrin repeat proteins probed by NMR. *J Mol Biol* 402(1):241–258.
2. Wetzel SK, Settanni G, Kenig M, Binz HK, Plückthun A (2008) Folding and unfolding mechanism of highly stable full-consensus ankyrin repeat proteins. *J Mol Biol* 376(1):241–257.
3. Forrer P, Chang C, Ott D, Wlodawer A, Plückthun A (2004) Kinetic stability and crystal structure of the viral capsid protein SHP. *J Mol Biol* 344(1):179–193.

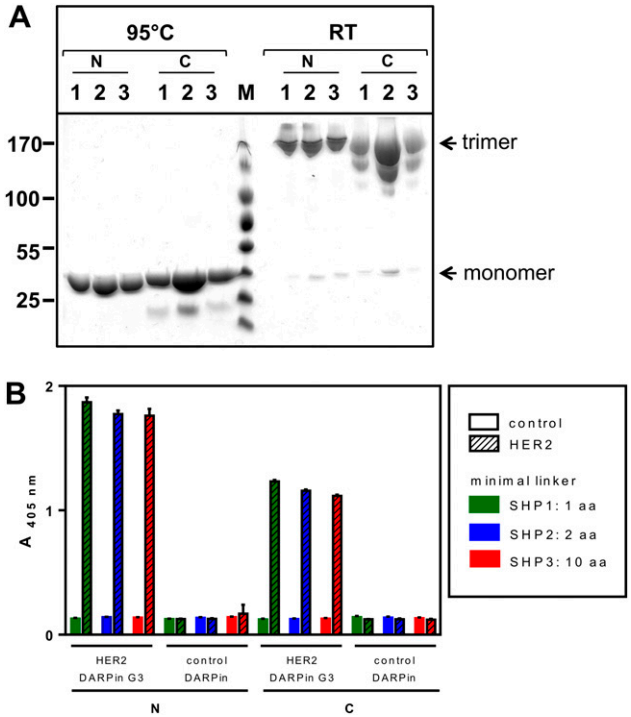

Fig. S6. Purity and oligomeric state of adapters. (*A*) Six micrograms of protein were loaded per lane and separated over a 10% SDS/PAGE gel. Samples were either boiled for 10 min (95 °C) or not boiled (RT). The gel was stained with Coomassie Brilliant Blue. Analysis was performed with adapters containing the knob-binding DARPin 1D3nc fused to the SHP with various linker lengths (1, 2, or 3; compare with Fig. 2 in the main text) and to the HER2-binding DARPin G3 at the N or C terminus, respectively. All adapters could be expressed and purified in the range of 50–100 mg/L culture in *Escherichia coli*. After two purification steps the adapters had a purity of >98%. The adapters formed stable trimers after expression as shown by the retention of the proteins without prior boiling (expected molar mass of the monomer, 43–44 kDa, depending on the linker) compared with the denatured samples (expected molecular weight of the trimer, 129–132 kDa, depending on the linker). (*B*) ELISA was performed to show simultaneous binding of HER2 and knob to the adapter either fused to the DARPin G3 (Her2-binding DARPin) or to the control DARPin E2_5. The tested adapters contained as the knob-binding module the knob-binding DARPin 1D3nc that was fused N-terminal of the SHP trimerization domain and was spaced by various amino acid lengths (minimal linker). The HER2-binding DARPin G3 or control DARPin E2_5 was fused at either the N terminus (N) or C terminus (C) of the knob-binding module. HER2 extracellular domain at a concentration of 10 nM was coated on a 96-well plate and incubated with 33 nM bispecific trimeric DARPin adapters. Before detection with streptavidin-AP, the biotinylated knob was incubated at a concentration of 100 nM. Adapters containing the HER2-binding DARPin G3 bound HER2 and knob simultaneously. Plain colored bars represent control. Hatched bars represent HER2-coated wells. The assays were performed in duplicate; error bars show the SD.

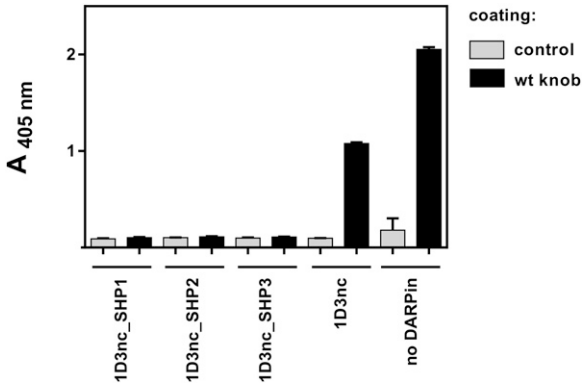

Fig. S7. ELISA for testing the binding of CAR to WT knob in competition with knob-specific DARPin fusion proteins. Biotinylated WT knob was immobilized via streptavidin (black bars), while only streptavidin-coated wells served as control (grey bars). Mixtures of 30 nM human CAR D1 domain fused to an HA tag were incubated with various knob-binding DARPin formats at a concentration of 100 nM (referring to the total concentration of binding sites in each construct). Several different knob-binding variants were investigated: the monomeric DARPin 1D3 with stabilized C-cap (1D3nc) and the trimeric DARPins containing 1D3nc and SHP with different linker lengths (SHP 1, 2, or 3). As a control, no DARPin was added to CAR D1, and binding to the WT knob defined the maximum signals that could be obtained with this experimental set-up. When the monomeric competitor 1D3nc was used, signals were reduced to ~50%. When the trimeric constructs (1D3nc_SHP) were used, signals returned to background levels. The monomeric DARPin 1D3nc has a K_d of ~1.0 nM, lower than the K_d reported for CAR D1 of 14.8 nM to the Ad5 knob (1). The trimeric knob-binding DARPins' greater binding success than CAR D1 can be explained by their increased valency and therefore improved functional affinity. These results indicate that CAR and knob-binding DARPin compete for binding to the knob, but they cannot bind simultaneously. The experiments were performed in duplicate; error bars show the SD.

1. Kirby I, et al. (1999) Mutations in the DG loop of adenovirus type 5 fiber knob protein abolish high-affinity binding to its cellular receptor CAR. *J Virol* 73(11):9508–9514.

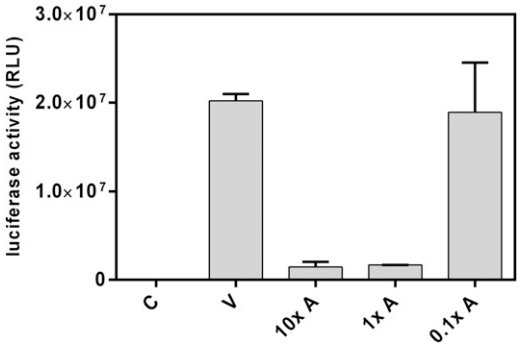

Fig. S8. Titration of fiber knobs with trimeric knob-binding DARPin blocking CAR-mediated infection of HEK293 Flp-In cells. One hundred virus particles (vp) per cell of Ad5luc virus coding for luciferase and containing the WT fiber knob domain (Ad5luc) was incubated with different molar ratios of 1D3nc_SHP1 trimeric knob-binder using a 10-fold excess (10× A), a 1:1 ratio (1× A), or a 0.1:1 ratio (0.1× A). HEK293 Flp-In cells were transduced. Relative luciferase light units (RLU) were determined 14 h after infection. The assay was performed in duplicate; error bars show the SD. Gene transfer was inhibited completely at a ratio of 1:1 (1× A) and could not be reduced further with a 10-fold excess of 1D3nc_SHP1 (10× A). This indication that all CAR-binding sites were blocked at a 1:1 ratio was consistent with the stoichiometry measured by SEC-MALS (Fig. S5). V, control transduction with virus alone, indicating maximum signals that can be obtained in this experimental set-up. C, background luciferase activity from noninfected cells.

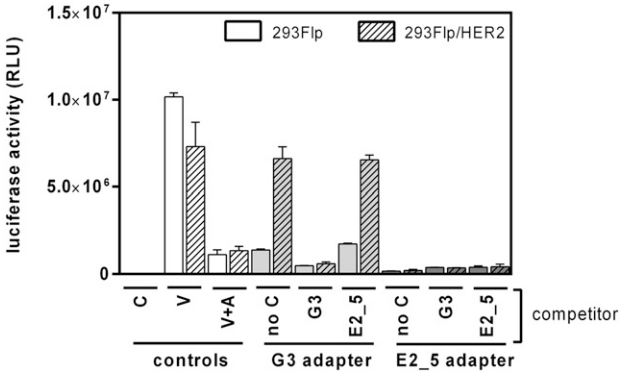

Fig. S9. Specificity of HER2-mediated transduction tested by competition. To show that entry of the adapters-virus complexes is HER2 specific, Ad5luc virus coding for luciferase and containing the WT fiber knob domain (Ad5luc) was coated with a 1:1 ratio of the knob-binding module (1D3nc_SHP1) with an N-terminal fusion of either the HER2-binding DARPin G3 (light gray bars) or a control DARPin E2_5 (dark gray bars). Before transduction, HEK293 Flp-In cells as control (plain bars) or cells stably overexpressing HER2 (hatched bars) were preincubated with no DARPin (no C), HER2-binding DARPin G3, or a control DARPin E2_5 at a concentration 0.5 μM for 1 h. Cells were harvested 14 h posttransduction, and luciferase activity was determined. The controls (white bars) show background activity (C), full infection at 100 vp per cell with virus alone (V), or non–CAR-related background signals with Ad5luc coated with 1D3nc_SHP1 not containing a retargeting module (V+A). The adapter containing E2_5 (dark gray bars) was not able to infect either cell line. When G3 was fused to the adapter, cells overexpressing HER2 showed luciferase activity in an HER2-dependent manner. This signal was reduced to background level when the competitor G3 was used but not when E2_5 was used. The assays were performed in duplicate; error bars show the SD.

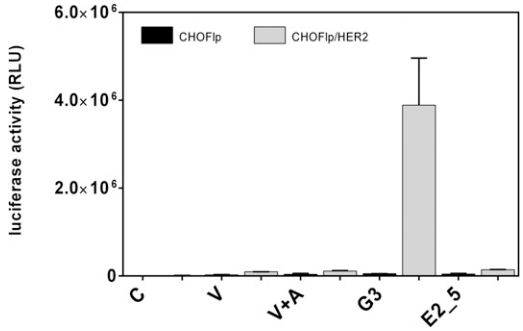

Fig. S10. Specificity of Ad5-mediated gene transfer in a HER2-dependent manner to CHO cells stably overexpressing HER2. Ad5luc virus coding for luciferase and containing the WT fiber knob domain (Ad5luc) at 100 vp per cell was preincubated with a 1:1 ratio of adapter to knob 1 h before transduction of the CHO cell line (black bars) or of CHO cells stably overexpressing HER2 (gray bars). The adapter 1D3nc_SHP1 was fused either to the HER2-binding DARPin G3 or to a control DARPin E2_5. Cells were harvested 16 h after transduction, and luciferase activity was measured. The G3-containing adapter was able to transduce CHO cells overexpressing HER2 35-fold over background compared with the control (V+A, see below), but not the control CHO cell line, whereas the control adapter containing DARPin E2_5 showed no significant transduction of either cell line. The controls show background activity (C), full infection at 100 vp per cell with uncoated virus (V), or non–CAR-related background signals with virus coated with a knob-binding module not containing a retargeting module (V+A). Because CHO cells do not express CAR, the signals for virus alone were only at background level. The assays were performed in duplicate; error bars show the SD.

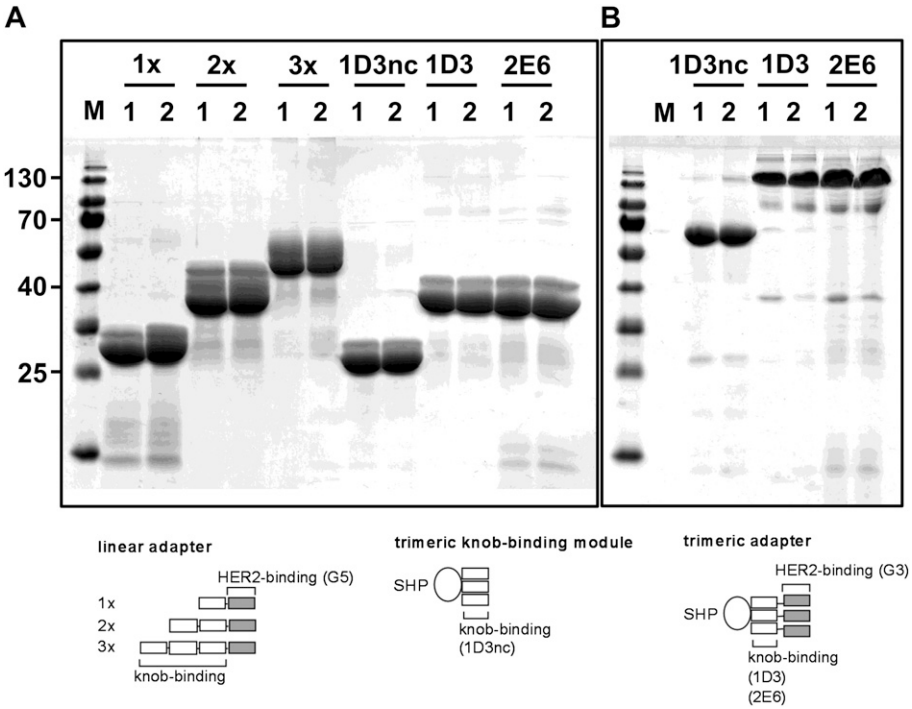

Fig. S11. Stability of adapters and competitors. Protein samples were incubated at room temperature for 2 wk (lanes 2) or freshly thawed from samples stored at −20 °C (lanes 1). Ten micrograms of protein were loaded per lane, separated over a 12% SDS/PAGE gel, and stained with Coomassie Brilliant Blue. 1×, linear bivalent adapter 2E6_G5; 2×, containing two knob-binding DARPins 2E6 $(2E6)_2$_G5; 3×, containing three knob-binding DARPins 2E6 $(2E6)_3$_G5 (1). 1D3nc, trimeric knob-binding DARPin 1D3nc_SHP1 (no retargeting module). Adapter 1D3 and 2E6, trimeric knob-binding DARPins 1D3nc_SHP1 or 2E6nc_SHP1 fused N-terminally with the HER2-binding DARPin G3. (*A*) Boiled samples. (*B*) Nonboiled samples. M, molecular weight marker (kDa). All adapters and the competitor tested showed no degradation over a time span of 2 wk when incubated at room temperature, compared with freshly thawed samples. The boiled samples ran at their expected molecular weight of 32 kDa for 2E6_G5, 48.7 kDa for $(2E6)_2$_G5, 65.8 kDa for $(2E6)_3$_G5, 28.3 kDa for 1D3nc_SHP1, 43 kDa for G3_1D3nc_SHP1, and 42.9 kDa for G3_2E6nc_SHP1. When the samples of the trimeric adapters and competitor were separated without prior boiling, the proteins showed a slower running band than the boiled samples with the molecular weight of 84.9 kDa for 1D3nc_SHP1, 129 kDa for G3_1D3nc_SHP1, and 128.7 kDa for G3_2E6nc_SHP1, indicating that they remained trimers over the course of the experiment.

1. Dreier B, et al. (2011) Her2-specific multivalent adapters confer designed tropism to adenovirus for gene targeting. *J Mol Biol* 405(2):410–426.

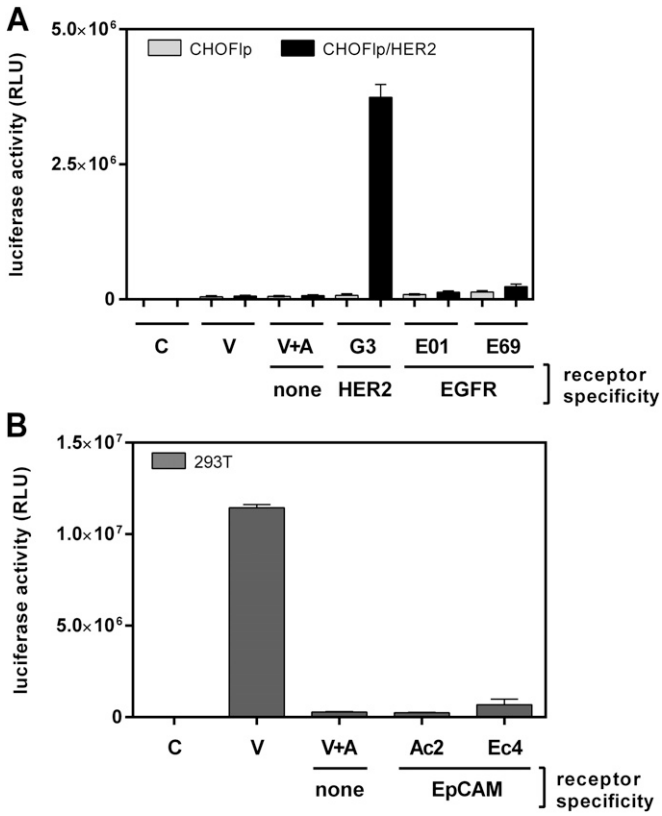

Fig. S12. Specificity of epidermal growth factor receptor) (EGFR) (*A*) and epithelial cell adhesion molecule (EpCAM) (*B*) adapters tested in cell lines not expressing these targets. As control, to test specificity of the EGFR and EpCAM adapters, they were incubated with Ad5luc virus coding for luciferase and containing the WT fiber knob domain (Ad5luc) at a ratio of adapter to knob of 1:1 and were used to transduce cell lines not expressing the respective target receptor. The controls denote background activity of cells alone (*C*), maximum infection at 100 vp per cell with virus alone representing the CAR-mediated entry for that respective cell line (V), or non–CAR-related background signals obtained with virus coated with the adapter 1D3_SHP1 not containing a retargeting module (V+A). (*A*) The CHO cell line (gray bars) or CHO stably expressing HER2 (black bars) was used as an EGFR-negative cell line. Ad5luc coated with an adapter fused to the HER2-specific DARPin G3 was able to infect only the HER2-overexpressing cell line. In contrast, when Ad5luc was coated with the EGFR-specific DARPins E01 or E69, no transduction was observed, as expected. Because CHO cells do not express CAR, the background activity with uncoated virus was very low. (*B*) For the EpCAM-specific adapters transduction to HEK293T, negative for EpCAM, were tested. The uncoated virus control (V) showed signals obtained by CAR entry, but both EpCAM-specific adapters containing Ac2 or Ec4 as the retargeting module, respectively, displayed only background signals. The assays were performed in duplicate; error bars show the SD.

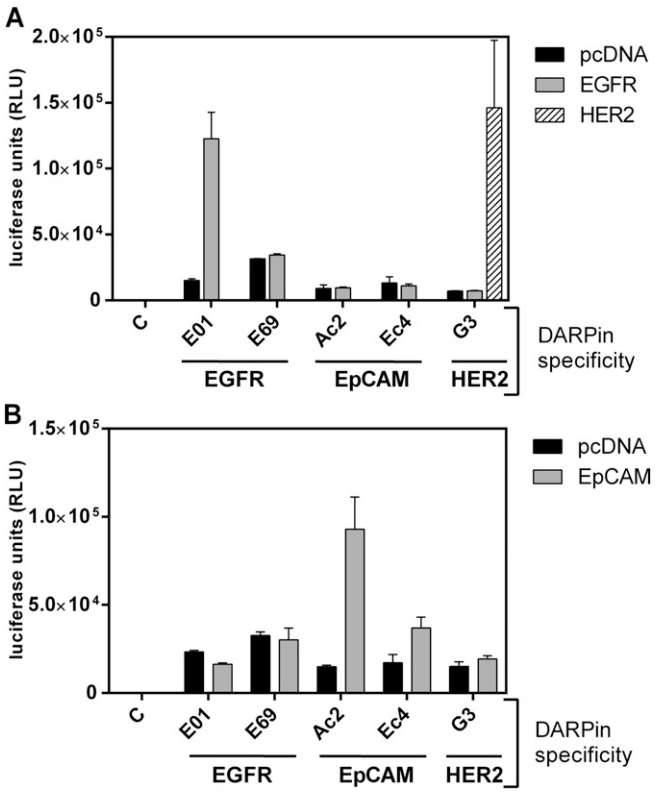

Fig. S13. Specificity of EGFR (*A*) and EpCAM (*B*) adapters tested in CHO Flp-In cells transiently expressing various cell-surface receptors. To test the specificity of the trimeric EGFR (containing either DARPins E01 or E69) and EpCAM adapters (containing either DARPin Ac2 or Ec4), CHO Flp-In cells were transiently transfected with constructs encoding for human EGFR WT, human EpCAM, or HER2. The trimeric adapter containing the DARPin G3 directed against HER2 was used as internal control for transfection. The adapters were incubated with adenovirus coding for luciferase and containing the WT fiber knob domain (Ad5luc) at a ratio of adapter to knob of 1:1. These coated viruses were used to transduce CHO Flp-In cells transiently transfected with eukaryotic expression plasmids encoding for the respective target receptor or the empty pcDNA3.1 as control at 100 vp per cell. Cells were harvested 14 h postinfection, and luciferase activity was determined. The controls denote background activity of cells alone (C). (*A*) CHO cells overexpressing EGFR were infected with Ad5luc coated with the trimeric E01 adapter luciferase activity eightfold over background corresponding to the pcDNA-transfected CHO cells but not to EpCAM-expressing cells. However, with the trimeric E69 adapter no significant infection was observed in this experiment, in contrast to high-expressing A431 cells (Fig. 6). This difference could be caused by several factors: (*i*) lower affinity of DARPin E69 of 15 nM vs. 0.5 nM of the DARPin E01 (1); (*ii*) low expression of EGFR in this experimental set-up compared with the expression on A431 cells used in Fig. 6*A* in the main text, which could result in reduced receptor cross-linking followed by reduced internalization; and (*iii*) accessibility of the epitope caused by a different glycosylation status in A431 tumor cells and nonhuman CHO cells. In contrast, CHO/HER2 cells showed luciferase expression 20.6-fold over background with Ad5luc coated with an adapter containing the HER2-specific DARPin G3 but not in cells transfected with empty pcDNA or EGFR. No transduction was observed with the EpCAM-specific adapters, as expected. (*B*) For the EpCAM-specific adapters Ac2 and Ec4 transduction of CHO cells transiently expressing EpCAM, luciferase expression was 6.2-fold or 2.2-fold, respectively, over that of cells transfected with empty pcDNA. No significant increase in luciferase expression was observed with the EpCAM-specific adapters E01 or E69 and the HER2-specific adapter G3, as expected. The assays were performed in duplicate; error bars show the SD.

1. Steiner D, Forrer P, Plückthun A (2008) Efficient selection of DARPins with sub-nanomolar affinities using SRP phage display. *J Mol Biol* 382(5):1211–1227.

Table S1. Data collection and refinement

Data collection	
Unit cell parameters	
a	109.6 Å
b	112.1 Å
c	129.67 Å
α	90°
β	90°
γ	90°
Space group	$P2_12_12_1$
Wavelength	0.9797 Å
Matthews coefficient*	3.39 $Å^3$/Da
Solvent content	63.38%
Resolution	1.95 Å (2.05–1.95 Å)
R_{sym}	4.6% (84%)
$I/\sigma^{\dagger}$	23.0 (2.90)
Completeness†	100% (100%)
Redundancy†	9.1 (9.05)
Wilson B-factor	35.4 $Å^2$
Refinement (Refmac 5.2.0019)	
Resolution range	46.57–1.95 Å
Completeness for range	100%
No. of reflections, working set	11,0875
No. of reflections, test set	5802
R_{work}	16.3%
R_{free}	19.3%
No. of protein atoms	7,757
No. of water molecules	735
RMS deviation of bond lengths	0.026 Å
RMS deviation of angle	2.35°
Overall mean B-factor	45.1 $Å^2$
Validation (Ramachandran plot)	
Residues in favored region	94.6%
Residues in allowed region	4.3%
Residues in outlier position	1.1%

*Calculated under assumption of a 3:1 (DARPin:knob) stoichiometry in the complex.

†Values in parentheses are data from the highest resolution shell.